Microwave Level Gauging System

by

Wei Guo

B.Eng, Tsinghua University, 1992

A Thesis Submitted in Partial Fulfillment of the
Requirements for the Degree of

MASTER OF APPLIED SCIENCE

in the Department of Electrical and Computer Engineering

We accept this thesis as conforming
to the required standard

[redacted]

Dr. S. S. Stuchly, Supervisor (Dept. of Elec. and Comp. Eng.)

[redacted]

Dr. A. Zielinski, Departmental Member (Dept. of Elec. and Comp. Eng.)

[redacted]

Dr. G. McLean, Outside Member (Dept. of Mech. Eng.)

[redacted]

Dr. D. J. Shpak, External Examiner (Royal Roads Military College, Victoria)

Supervisor: Dr. S. S. Stuchly

ABSTRACT

Two types of surface waveguides, the Goubau line and the dielectric rod, are considered as the transmission media for a microwave level gauging system for measurement of the liquid levels. Surface waveguides are capable of overcoming some limitations of the transmission media in the present systems. They are free from the parasitic reflections from surrounding objects, which is the main problem in the system utilizing free space propagation, and are resistant to the deposits which may degrade the performance of systems with metallic waveguides. An experimental arrangement is developed and the operation of the system is verified by the measurements of the actual levels of water and oil. Both theoretical studies and experimental results show that the surface waveguides maybe suitable as the transmission media for a microwave level gauging system.

Examiners

[redacted]

Dr. S. S. Stuchly, Supervisor (Dept. of Elec. and Comp. Eng.)

[redacted]

Dr. A. Zielinski, Departmental Member (Dept. of Elec. and Comp. Eng.)

[redacted]

Dr. G. McLean, Outside Member (Dept. of Mech. Eng.)

[redacted]

Dr. D. J. Shpak, External Examiner (Royal Roads Military College, Victoria)

Table of Contents

List of Tables

List of Figures

Acknowledgments

I would like take this opportunity to thank my supervisor, Dr. S. S. Stuchly, for his advice during my whole research and study of M. A. Sc program at the University of Victoria. Dr. S. S. Stuchly suggested this research topic. I am grateful to him for his continuous guidance, encouragement and seemingly endless patience throughout the development of this thesis. I am also grateful to him for his financial support to make it possible to finish my M. A. Sc program and this thesis.

I would also like to thank Dr. M. Bialkowski, Professor of the Department of Electrical and Computer Engineering, University of Queensland, Australia, Mr. K. Caputa and Dr. M. Okoniewski for their kindly assistance in developing the experimental system arrangements and their valuable suggestions for the experimental work.

In addition, I would also like to thank Dr. A. Zielinski and Dr. G. McLean for serving on my supervisory committee, providing valuable suggestions, kindly assisting and patiently reviewing this research throughout my M. A. Sc program.

Finally, I would like to thank the faculty members and staff at the Department of Electrical and Computer Engineering, University of Victoria, from whom I got much help.

Chapter 1

Introduction

1.1 Level measurement

Measuring and controlling the level of liquids contained in storage and processing vessels is important in modern industrial processes. In the case of storage tanks, one is usually dealing with large volumes of often expensive products. The liquids which require level measurements range from pure water to viscous, corrosive, flammable, sticky fluids and sherries. The processing environments for level sensors extend from vacuum to high pressure environments, and from subzero to elevated temperature [1]. The interfaces encountered in the measurements include air to liquid, air to foam, foam to liquid and others[2]. Figure 1.1 depicts the problems that need to be addressed in closed metal tanks [3].

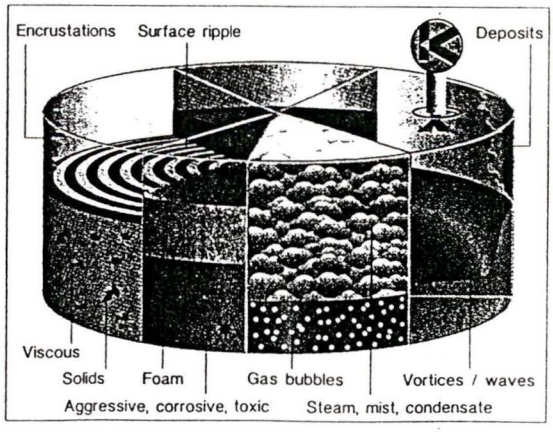

Figure 1.1 Closed vessel level sensing [3]

Level measurement requirements in tanks often exceed those in ordinary process level measurements and a large number of level measuring techniques have been developed. Basically, they fall into four categories: mechanical, pneumatic, electrical and electronic techniques.

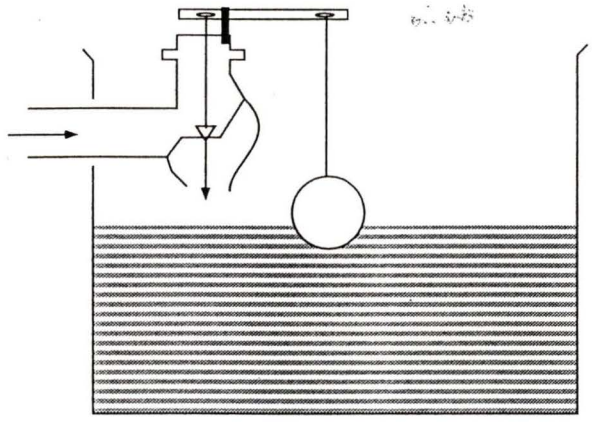

Figure 1.2 Schematic diagram of a mechanically operated float valve [1]

Figure 1.2 shows a schematic diagram of a mechanically operated float-valve system [1]. In this device, the float directly positions a valve mechanism to open and close it and allows more or less flow of liquid into the vessel. These devices have been widely used for measurement and control of levels in hot wells, storage tanks and stills. One of the limitations of such device is that when the float device is located in the vessel, repair or maintenance while the unit is in operation can not be made.Moreover, due to the limitations of the diameter of the float, the range of level measurements is usually limited.

The electrical capacitance effect has also been used for level measurement. In such a system, the capacitance of a suitable sensing element varies with the level of the material, and measurement of this capacitance gives a direct reading of the level [1]. For a capacitance system, the structure of the primary sensing element is very simple and rugged. Capability for temperature, pressure, and corrosion resistance is easily obtained. The cost of most capacitance system is competitive with that of the simple mechanical

units. The major limitation of capacitance system is that it is not suitable for measuring liquids whose dielectric constant changes with temperature or for viscous conducting liquids which coat the sensing element and can cause erroneous readings. The bubbles in the liquid or foam on top of the liquid can also cause errors.

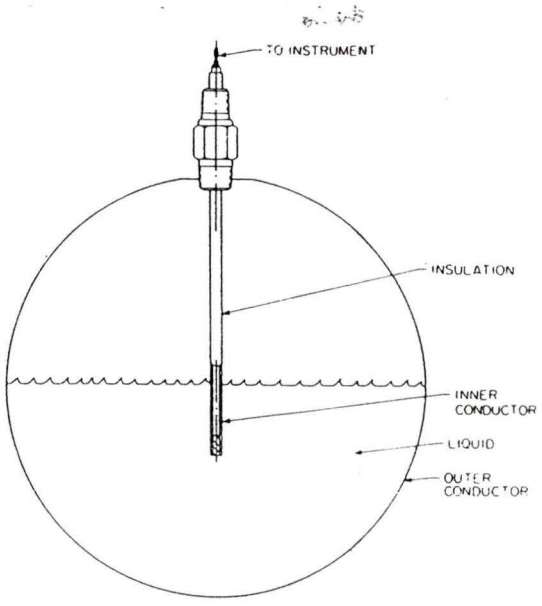

Figure 1.3 Capacitance probe installation [1]

The sensors in mechanical and electrical systems directly contact with the measurement liquids. The measurement accuracy is usually independent of the processing environment such as fog, dust or vapor and measurement interface. However, contacting sensors are not suitable for corrosive and high temperature (molten metal) products. To meet the requirements for chemical and steel industry applications, a number of non-contacting level gauging system have been developed[10].

Sonic and ultrasonic techniques are the earliest non-contacting techniques for level measurement. The principle is to measure the transit time between a sonic wave transmitter and a receiver. A continuous sonic-type level measuring unit is shown in Fig. 1.4 [1]. The limitation of such a system results from the fact that environmental changes which affect the velocity of acoustic propagation, on which the measurement is fundamentally

based, can influence the measurement accuracy. Notably, these changes are temperature, pressure, or chemical composition.

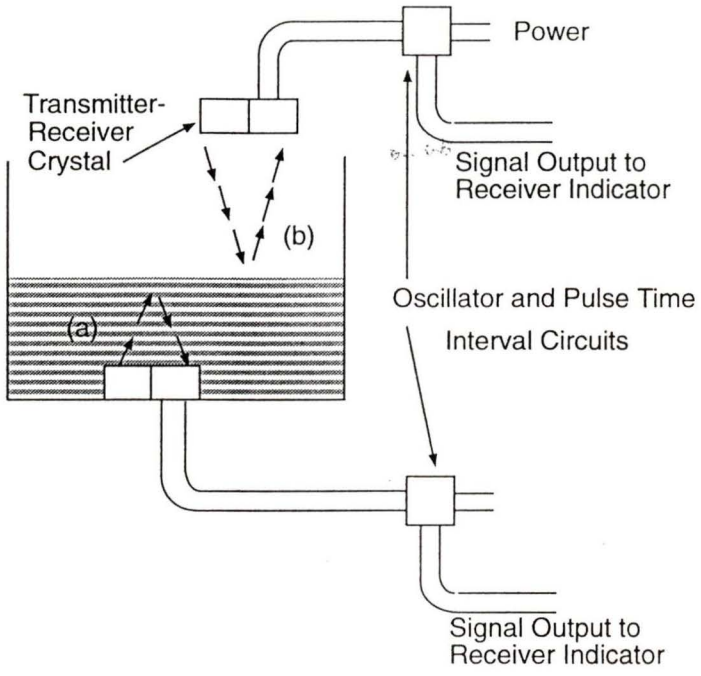

Figure 1.4 Continuous sonic-type level measuring unit. (a) Liquid phase, (b) vapor phase [1]

Laser level gauging systems offer the most accurate measurements. But such accuracy requires a good processing environment and highly reflective products. Laser radiation cannot penetrate the vapor, dust, smoke and flying debris which might cover the liquids. Furthermore, the intensity of the reflected signal depends on the properties of the liquids. For some kinds of chemical compositions or black liquids, the echo signal is too weak to make the level system work effectively.

1.2 Microwave level gauging system

Microwave techniques appear to be an ideal solution for closed vessels. Actually, microwave techniques for level measurement have been used in marine applications and coal storage for many years. Limited by the high price of hardware, microwave techniques were not applied to land-based storage tanks for level measurement until the last decade [2].

The principle of operation is quite straightforward. The gauge antenna radiates the electromagnetic wave, whose propagation velocity is v, and the time period during which the wave travels from transmitter to the level surface t is measured. Then, the level can be calculated by $R = vt/2$. Figure 1.5 shows a schematic of a microwave level gauge system.

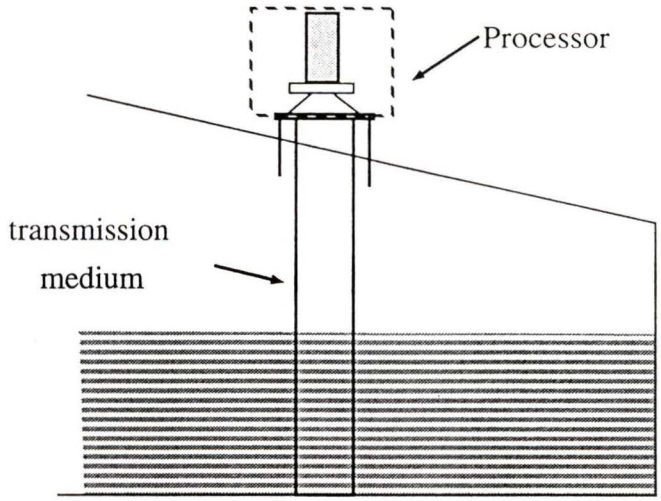

Figure 1.5 An example of microwave level gauge system

It consists of two main parts: the processor unit and the transmission medium. The processor unit is for transmitting the electromagnetic wave as well as for processing the received echo signal to get the level information. The transmission medium is the path for EM waves to reach the target and return back to the transmitter.

Compared with other techniques, microwave has the following advantages:

1. Suitable for working under harsh environments. The use of electromagnetic waves makes it possible to work in vacuums as well as being independent of the pressure in the process vessel. Moreover, it is not influenced by noise, dust, or high temperature which make optical and infrared techniques fail.
2. Suitable for on line, continuous monitoring.
3. A highly reflective target is not needed, unlike optical techniques.
4. Inert to the process environment.
5. Capable of ignoring the disturbing features like a rotating agitator, blades, struts, rivets, heater coils.
6. Capable of providing both contacting systems and non-contacting systems for different applications.

Recently, two schemes have been developed for microwave level gauging systems:

1. Free-space propagation with frequency-modulation continuous-wave (FMCW) technique
2. Circular waveguide propagation with multiple-frequency continuous-wave (MFCW) technique

The first scheme is shown in Fig. 1.6 [4]. It can carry out non-contact monitoring and requires simple hardware. The drawback is that it suffers from parasitic reflections, which degrade the sensitivity and accuracy of the system.

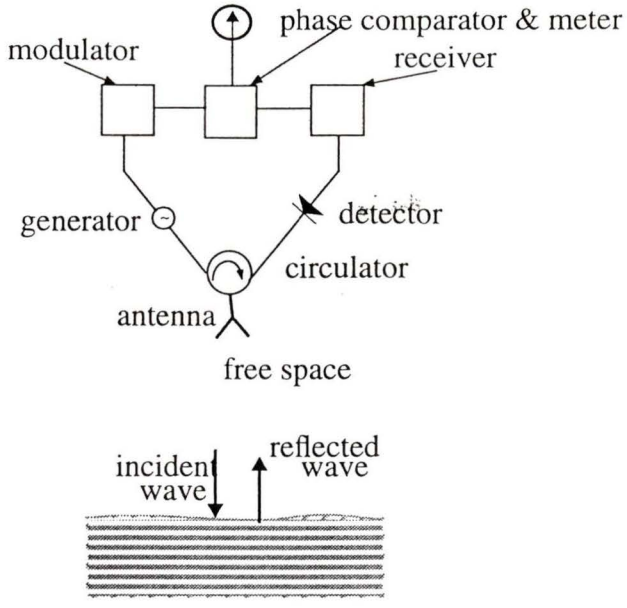

Figure 1.6 Free space propagation scheme [4]

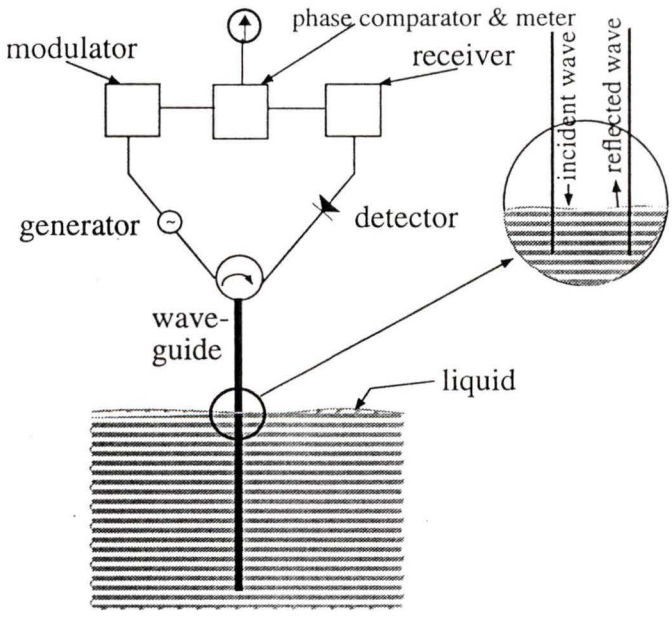

Figure 1.7 Waveguide propagation system [4]

Figure 1.7 depicts the principle for a waveguide propagation system [4]. For such systems, the EM waves transmitted by the processing unit propagate along a section of

circular waveguide. In contrast to the free-space propagation, it is free from parasitic reflections. The sensitivity and accuracy are therefore better than for free space propagation. However, the closed boundary structure of the waveguides induces the meniscus effect which reduces the measurement accuracy. Any deposits on the inside wall of the waveguides also introduce measurement errors. Furthermore, the waveguide increases the complexity of the hardware and difficulty of installation.

1.3 Overview of the thesis

From the above discussions, it is clear that the limitations of the propagation media limit the applications of microwave level gauging systems. The objective of this thesis is to investigate a new transmission medium which can utilize the advantages of both free space and metallic waveguides for the microwave level gauging system.

Chapter 2 commences with the principles of microwave techniques for distance measurement. Both time-domain as well as frequency-domain techniques are introduced in this chapter and a brief perspective discussion is also presented.

The theory of surface waveguides, which is investigated as the transmission medium for the microwave level gauging system, is introduced in Chapter 3. It is very important as it is the basis of the total system. As potential transmission media, two kinds of surface waveguides, the dielectric rod and the Goubau line, are investigated. A comparison of surface waveguides and commonly used transmission lines is also given in this chapter.

Chapter 4 describes the experimental arrangements and the experimental results of the total system. The conclusions for the investigated surface waveguide system, including feasibility, advantages, and disadvantages as well as a comparisons with existing systems, are presented in Chapter 5.

Chapter 2

Microwave techniques for level gauge

Level measurements are in fact measurements of the distance from a liquid surface to a reference point. As mentioned in chapter 1, if the propagation velocity of EM wave v is known, and the time period t during which the EM wave travels from the substance level to the reference point and back is measured, the level can be obtained from $R = vt/2$. In this chapter, several microwave techniques for level measurement are introduced.

2.1 Time domain techniques

Time domain techniques involve direct measurement of the time period t. They include (1) determination of the time period t by comparing the transmitted and echo pulse signals (pulse radar); and (2) determination of the time period t by the interference pattern of the transmitted and received step signals (TDR).

2.1.1 Pulse radar

Pulse radar transmits a periodic train of short pulses and measures the time difference between the transmitted and received pulses [5]. As shown in Fig. 2.1, the pulse duration is τ, and the pulse repetition frequency $f_T = 1/\tau_T$. The transmitted wave covers the distance R between the radar and target, and returns towards the radar with time delay τ_{ar}. So,

$$R = v \times \tau_{ar}/2 \ . \tag{2.1}$$

As shown in Fig. 2.1, if $\tau_{ar} < \tau$, we can not distinguish the transmitted and the echo

pulses. The resolution of distance measurement for pulse radar is

$$R_{min} = \frac{v\tau}{2}. \tag{2.2}$$

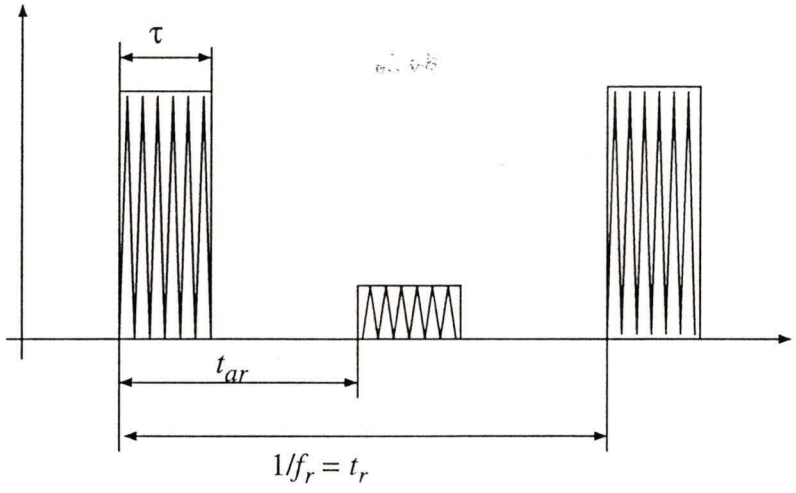

Figure 2.1 Principle of pulse radar [5]

The shorter the pulse duration is, the better the resolution will be. However, typically this requires faster electronic and emits a lower power. Moreover, in practice, since the pulse envelope is not the ideal square one, the resolution also depends on the pulse start time (rise time) and pulse stop time (fall time).

2.1.2 Time domain reflectometry (TDR)

A time domain reflectometer (TDR) utilizes a step signal to display the response of a system. As shown in Fig. 2.2, from the interference pattern of the incident and reflected waves, we can obtain the time delay T and therefore the distance to the reflection may be deduced as [7][8]

$$x - x_0 = \frac{vT}{2} \tag{2.3}$$

where x is the location of discontinuity and x_0 is the location of reference plane

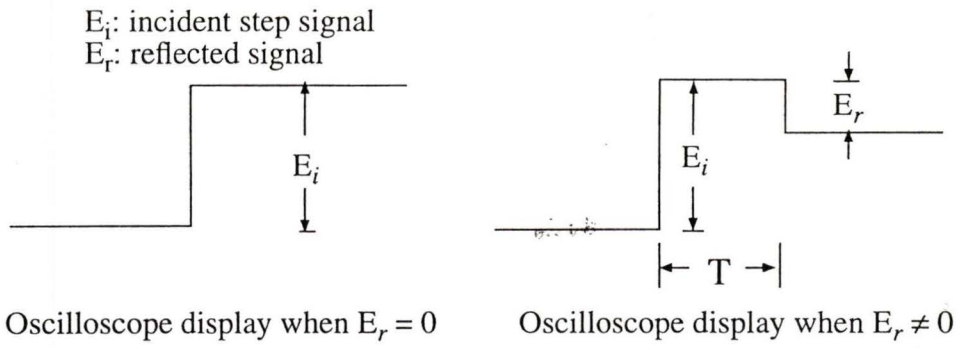

Figure 2.2 Interference pattern in the step signal [7]

Also, from the amplitude and waveform of the reflected signal, we may obtain the nature (resistive or reactive) of the discontinuities. A TDR system for short distance measurement is shown in Fig. 2.3.

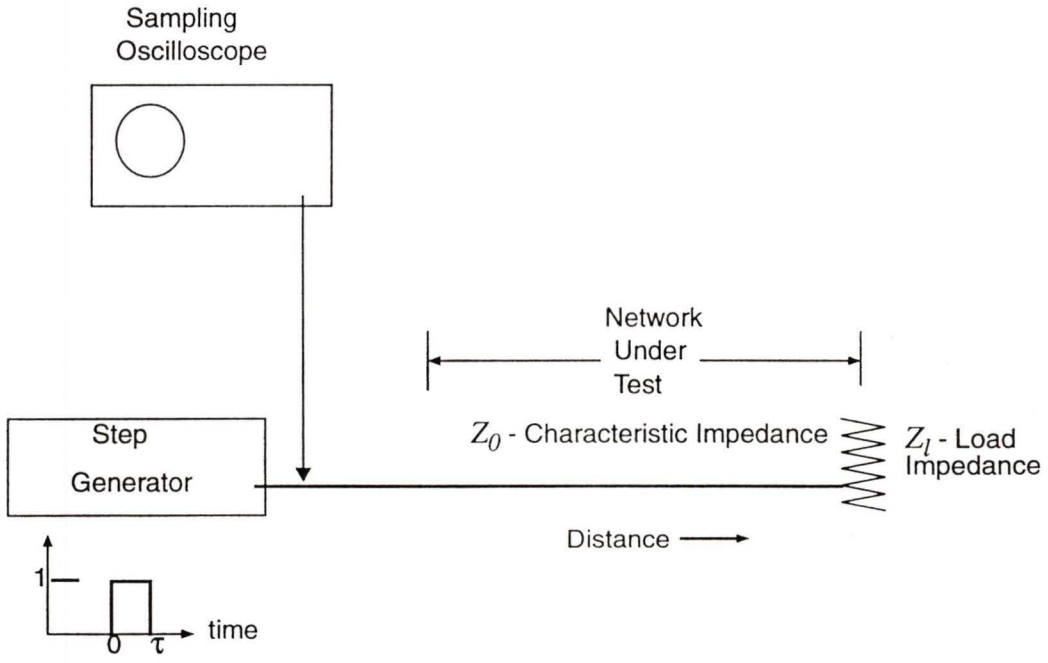

Figure 2.3 A time domain reflectometer for distance measurement [7]

From above discussions, we know that the time domain techniques use the leading edge of the pulse or step signal to obtain distance information. The measurement accu-

racy and resolution are determined by the rise and/or fall time of the transmitted signals. Since pulse and step signals are utilized, the spectra are very broad and thus non-dispersive components are required for the system. Therefore, instead of being used for level gauge, time domain techniques are more often used for long distance measurements and the detection of the discontinuities in transmission lines.

2.2 Frequency-domain techniques

Frequency-domain techniques utilize parameters which are related to the time period *t*. Basically, they include: (1) measurements of the phase difference between transmitted and reflected continuous-wave (CW) signals; (2) measurement of the frequency shift between the transmitted and reflected swept signals;

First, let us consider a single CW radar. If the transmitted signal is

$$V_t = \sin 2\pi f_0 t \tag{2.4}$$

and the travel time is *T*, the echo signal is

$$V_r = \sin\left[2\pi f_0 (t - T)\right] \tag{2.5}$$

Mixing the received echo signal and the transmitted signal with a phase detector, we can obtain the phase difference as

$$\Delta\phi = \frac{4\pi R}{\lambda} \tag{2.6}$$

where λ is the wavelength of the transmitted signal and therefore the distance R is

$$R = \frac{c\Delta\phi}{4\pi f_0} = \frac{\lambda}{4\pi}\Delta\phi \tag{2.7}$$

where c is the velocity of free space propagation

In the practical measurement, the output of the phase detector can not exceed 2π radians. Substituting $\Delta\phi=2\pi$ into (2.7) gives the maximum unambiguous range as

$$R_{max} = \frac{\lambda}{2} \tag{2.8}$$

At microwave frequencies, this unambiguous range is far too small to be of practical interest. This inability results from the relative narrow bandwidth of the transmitted waveform of CW radar [9]. Two kinds of technique have been developed to solve this problem:

1. MF-CW technique
2. Swept frequency techniques

2.2.1 MF-CW technique

Utilizing two separate CW signals slightly differing in frequency, the region of unambiguous range for CW radar can be extended. The unambiguous range in this case corresponds to a half wavelength at the difference frequency [4][9].

The transmitted waveform is assumed to consist of two continuous sine waves of frequency f_1 and f_2 separately by an amount of Δf.

$$V_{1t} = \sin(2\pi f_1 t + \phi_1) \tag{2.9}$$

$$V_{2t} = \sin(2\pi f_2 t + \phi_2) \tag{2.10}$$

where ϕ_1, ϕ_2 are arbitrary (constant) phase angles.

The echo signals are

$$V_{1r} = \sin\left(2\pi f_1\left(t - \frac{2R}{v}\right) + \phi_1\right) \tag{2.11}$$

$$V_{2r} = \sin\left(2\pi f_2\left(t - \frac{2R}{v}\right) + \phi_2\right) \tag{2.12}$$

where v is the propagation velocity of the transmitted signals

The receiver separates the two components of the echo signals and heterodynes

each received signal component with the corresponding transmitted waveform. So, distance R is

$$R = \frac{c\,(n_1 + \Delta\phi_1)}{4f_1} \tag{2.13}$$

$$R = \frac{c\,(n_2 + \Delta\phi_2)}{4f_2} \tag{2.14}$$

where n_1, n_2 are integers

$\Delta\phi_1$, $\Delta\phi_2$ are the phase difference between V_{1t}, V_{1r} and V_{2t}, V_{2r}, respectively.

Hence,

$$R = \frac{c\,(n_2 - n_1 + \Delta\phi_2 - \Delta\phi_1)}{4\,(f_2 - f_1)} \tag{2.15}$$

Only if n_2 - n_1 = 0 and $\Delta\phi_1$ - $\Delta\phi_2 < 2\pi$, does the measured distance remain unambiguous. Therefore, the range is

$$R = \frac{c\Delta\phi}{4\pi\Delta f} \tag{2.16}$$

and the maximum unambiguous range is

$$R_{max} = \frac{c}{2\Delta f} \tag{2.17}$$

A large Δf improves the accuracy of the range measurements since a large Δf means a proportionately large change in $\Delta\Phi$ for a given range. However, there is a limitation to the value of Δf in order to be measured unambiguous. The maximum Δf is

$$\Delta f_{max} = \frac{c}{2R_{max}} \tag{2.18}$$

So, if we only use Δf to measure the distance, there exists a trade-off between measurement accuracy and unambiguous range.

If we use Δf to determine the unambiguous range and then use one of the two fundamental frequencies to improve the accuracy, both high accuracy and large unambiguity can be obtained. For example, we choose f_1 and f_2 as 9.99 GHz and 10 GHz respectively, the unambiguous range $R_{max} = \frac{c}{2\Delta f} = 15m$. Assume the measurement uncertainty of phase detector is $\pm 1.5^{o}$. When Δf is used for the distance measurements, the level measurement error due to the phase measurement uncertainty is δR = 41.7 mm. If f_2 = 10 GHz is then used, δR is 0.0312 mm. Thus, we reduce the measurement error and maintain the unambiguous range.

The above analysis was made by choosing the microwave carrier as the fundamental frequency. We can also use amplitude modulation (AM) signal to realize a similar principle. In the AM case, one frequency is the carrier f_c and another frequency is the modulation frequency f_m. The modulation frequency f_m is used to determine the unambiguous range of the measured distance and the carrier frequency f_c is used to determine the accuracy.

2.2.2 Swept-frequency techniques

Another way to increase the spectrum of the transmitted signal is to use a swept frequency - that is, the frequency of the transmitted signal is swept/stepped across a certain bandwidth. The swept frequency techniques include:

1. FM-CW technique
2. Frequency response technique
3. Direct phase measurement technique
4. Stepped frequency reflectometry
5. Direct timing technique

2.2.2.1 FM-CW technique

In frequency-modulated continuous-wave (FMCW) technique, the frequency of transmitted signal increases linearly with time [9]. If the distance between the transmitter and target surface is R, an echo signal returns after a time $T = 2R/c$ and the echo signal is mixed with a portion of the transmitted signal in a nonlinear element, then, a beat frequency f_r will be produced as

$$f_r = \dot{f}_o T = \frac{2R}{c}\dot{f}_o \tag{2.19}$$

where $\dot{f}_0$ is the rate of change of the carrier frequency.

In any practical case, the frequency can not be continuously changed in one direction only. Periodicity in the modulation is necessary, as in the triangular-frequency-modulated waveform shown in Fig. 2.4.

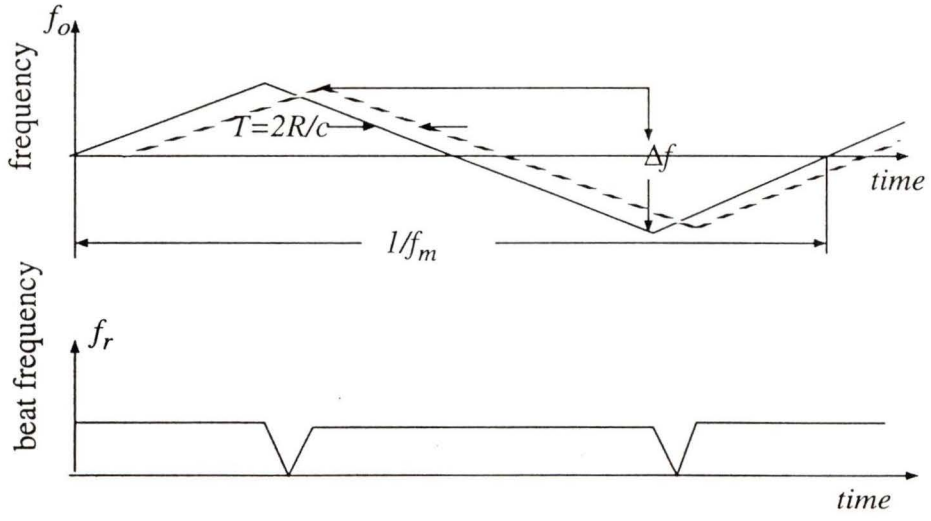

Frequency-time relationships in FM-CW technique. solid curve represents transmitted signal; dashed curve represents echo

Figure 2.4 Triangle-waveform modulation [9]

For triangular modulation, the beat frequency is of constant frequency except at the turn-around region. If the frequency is modulated at rate f_m over a range Δf, the beat frequency is

$$f_r = \frac{2R}{c} 2 f_m \Delta f \tag{2.20}$$

So,

$$R = \frac{f_r c}{4 f_m \Delta f} \tag{2.21}$$

where f_r is the beat frequency, f_m is the modulation rate and

Δf is the frequency deviation

Therefore, the beat frequency determines the range R. If non-linear modulation is used, it was shown that (2.21) also yields a correct result provided that the average beat frequency measured over a modulation cycle is used.

The FM-CW technique can be used to measure short as well as long distances. It has no minimum range as that in the time domain pulse technique. The unambiguous range is determined by the frequency modulation rate f_m. Usually, f_m is very small and the unambiguous range is very large.

The measurement accuracy of the FM-CW system is often limited by two factors: (1) the uncertainty of the beat frequency measurement which is imposed by the phase detection hardware in the receiver; (2) the undesirable multiple reflections (clutter) resulting from the surrounding objects. With a highly accurate phase detector, the error caused by the first factor can be reduced to a negligible level [10].

Restricted by the dispersion of most transmission media, FMCW systems often adopt free space propagation and thus the unwanted multiple reflections caused by the surrounding objects are inevitable. Such multiple reflections will severely distort the waveform of the non-linear (mixer) output and degrade the measurement accuracy. For example, the mixer output without multiple reflections is a sinusoidal function as shown in Fig. 2.5(a). If there are multiple targets between the transmitter and receiver, the wave-

form corresponding to the target will be modulated by other frequencies resulting from the surrounding objects. Figure 2.5(b) shows the mixer output when a second object exists.

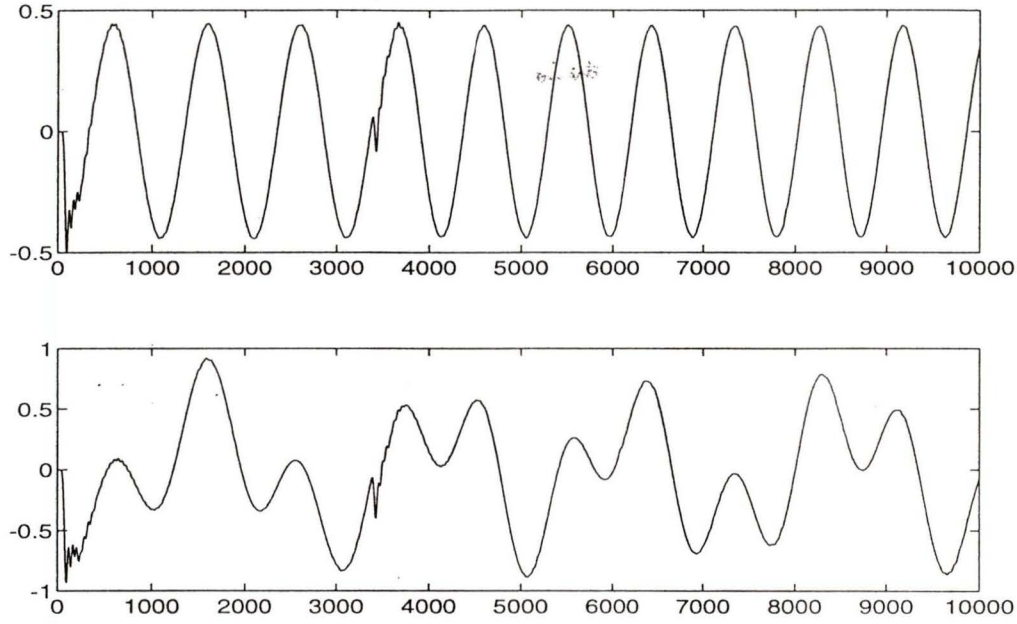

Figure 2.5 (a) Output of the phase detector for the only target, (b) output of the phase detector when the second objective exists

In order to reduce the measurement uncertainty caused by the clutter and improve the Signal to Noise Ratio (SNR) of the received signal, advanced signal processing techniques have to be used. A computer controlled spatial filter is reported to be successfully adopted in a FMCW/CW system [10]. Based on the fact that different object corresponds to different frequency component in the mixer output, the spatial filter is realized by a narrow band adaptive filter centered about an estimate of the current target range. This approach has the advantage of attenuating the clutter everywhere except very close to the primary target. A block diagram of the adaptive filter is shown in Fig. 2.6(a). This type of filtering was found to provide excellent rejection of extraneous reflections as can be seen in Fig. 2.6 (b) and (c).

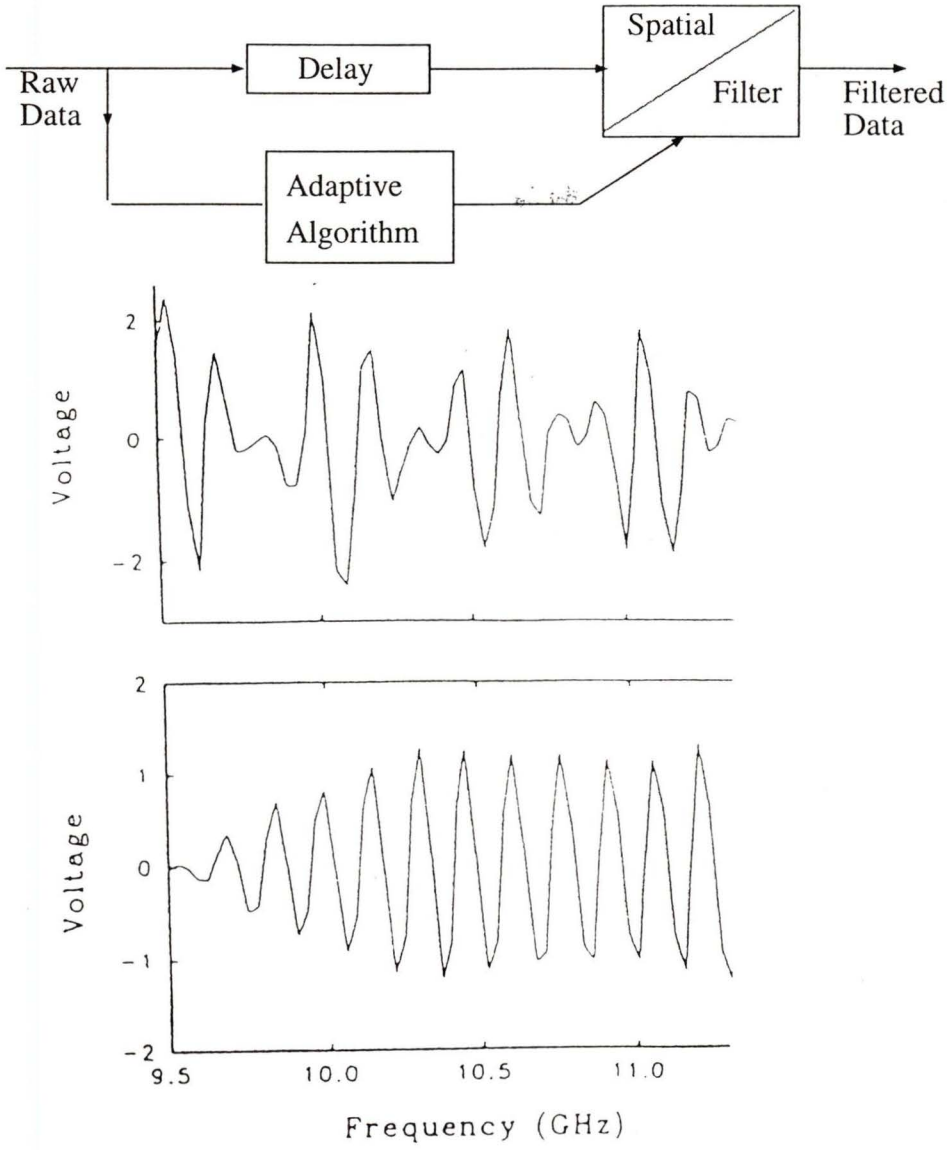

Figure 2.6 (a) Adaptive spatial filter block diagram, (b) unfiltered response at output of phase detector with main target at 50 cm and a smaller secondary target at 20 cm (c) filtered response

Furthermore, to be compatible with the computer, the frequency of the transmitted signal steps instead of sweeping in a certain bandwidth. The diagram of the total reported system is shown in Fig. 2.7 and Fig. 2.8 gives the comparison of the measurement accuracy between general FMCW and processed FMCW systems. We can see that the worst case error for processed FMCW system is less than 0.4 cm.

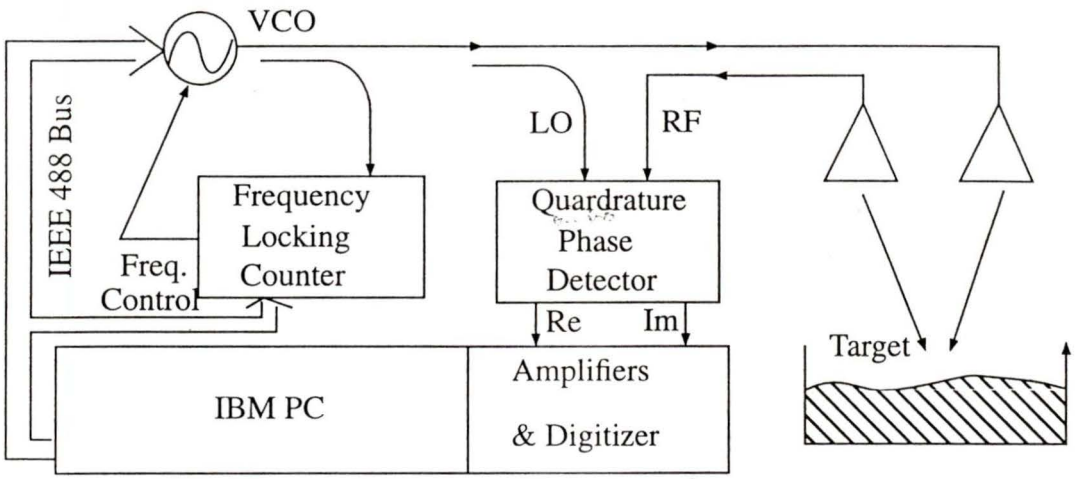

Figure 2.7 Diagram of FMCW/CW system

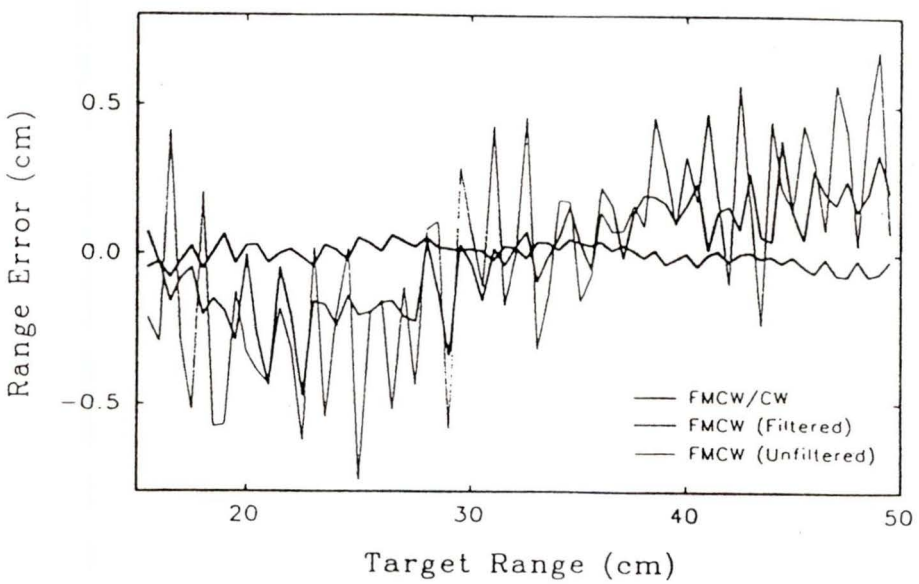

Figure 2.8 Comparison of the measurement accuracy between three FMCW techniques

2.2.2.2 Frequency response techniques

The initial purpose of this technique is to detect the discontinuities along a transmission line, especially in the cases when the TDR method fails. It utilizes the principle that the Fourier transform of the reflection coefficient, which is a function of frequency, implies the distribution of the discontinuities of a transmission line system [13].

Figure 2.9 shows the general block diagram for a transmission-line system with discontinuities. Every 2-port of infinitesimally small electrical length is followed by a transmission line of electrical length (x_{i+1} - x_i) and characteristic impedance. Therefore, the complex reflection coefficient at position x be written as

$$r(x,f) = \frac{V_R}{V_I} \tag{2.22}$$

where V_I is the complex modulus of the incident voltage wave at x, and V_R is the complex modulus of the reflected voltage wave at x

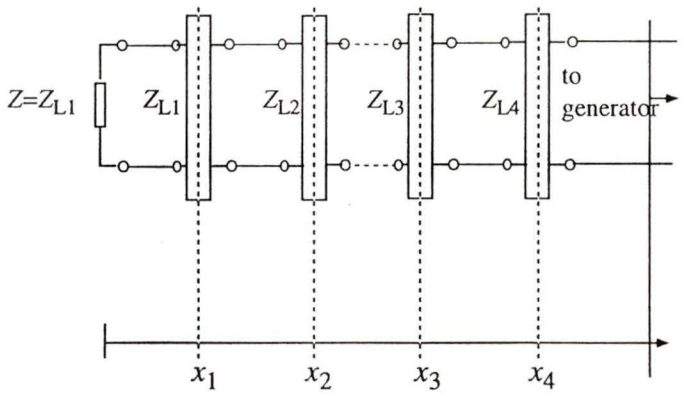

Figure 2.9 Block diagram for a transmission line system with discontinuities [10]

The incident voltage wave V_{Ii} is approximately not influenced by propagating the 2-port i, but every 2-port is the source of a reflected wave V_{Ri}. Applying the transmission-line formula, V_I and V_R turn out to be

$$V_I(x,f) = V_0 exp\{j\beta(x-x_0)\} \tag{2.23}$$

$$V_R(x,f) = \sum_{i=1}^{k} V_{Ri} exp\{-j\beta(x-x_i)\} \tag{2.24}$$

where $\beta = 2\pi/\lambda = 2\pi f/c$, c is the velocity of propagation and

k is the value that x_k is the largest x_i which is just smaller than x.

If we define $R_i = V_{Ri}/V_{Ii}$, the reflection coefficient of a 2-port discontinuity terminated by its characteristic impedance, $r(x,f)$ may be written

$$r(x,f) = \sum_{i=1}^{L} R_i \gamma(x-x_i) exp\{-j2\frac{2(x-x_i)}{c}f\} \tag{2.25}$$

where $\gamma(x)$ is the step function.

The function $r(x,f)$ generally characterizes the response of the reflection coefficient as a function of position and frequency. By choosing $x=x_0 > x_L$, $r(x,f)$ becomes the input reflection coefficient of the transmission-line system with a reference plane at position x_0. Then, (2.25) can be written

$$r(x_0,f) = r(f) = \sum_{i=1}^{L} R_i exp\{-2\pi j\frac{2(x_0-x_i)}{c}f\} \tag{2.26}$$

where $r(f)$ depends on frequency. The inverse Fourier transform is applied to $r(f)$ to transform $r(f)$ into the time domain. The result, which may be called $R'(t)$, is the impulse response of the unknown transmission-line system as a function of time at position x_0.

$$R'(t) = \int_{-\infty}^{+\infty} r(f) exp(j2\pi tf)\, df \tag{2.27}$$

Assuming the value of R_i to be independent of frequency, $R'(t)$ may be written

$$R'(t) = \sum_{i=1}^{L} R_i \delta \{ t - \frac{2(x_0 - x_i)}{c} \} \tag{2.28}$$

The impulse response consists of serval unit impulses $\delta(t)$ occurring at the instants of time $t_i = 2(x_0\text{-}x_i)/c$. Every unit impulse at time t corresponds to a discontinuity at position x. Therefore,

$$x = x_0 - \frac{ct}{2} \tag{2.29}$$

In practice, the frequency domain in which $r(x, f)$ can be measured is finite and may range from $f = F_0 - \Delta F$ to $f = F_0 + \Delta F$. Transforming $r(x, f)$ into the time domain by the finite Fourier transform, we obtain

$$R'(t) = \int_{F_0 - \Delta F}^{F_0 + \Delta F} r(f) \exp(j2\pi tf)\, df \tag{2.30}$$

$$R'(t) = 2\Delta f \sum_{i=1}^{L} R_i \frac{\sin \{ 2\pi \Delta F \frac{2(x - x_i)}{c} \}}{2\pi \Delta F \frac{2(x - x_i)}{c}} \exp \{ -j2\pi F_0 \frac{2(x - x_0)}{c} \} \tag{2.31}$$

Comparing (2.31) with (2.28), it is evident that, by changing to a limited frequency range, the unit impulses change to functions of the form $sin(x)/x$, the main lobes of which are located at the positions of the original unit impulses.

Although above analysis refers to detecting discontinuities along a transmission line, obviously the same principle can be applied to level measurement. In level measurement, what we want to measure is the distance between the transmitter and the target surface. So, the target surface now is the discontinuity and by applying the above principle to it, we can locate the target and thus the distance. As an additional advantage, the capability of detecting multiple discontinuities of this technique can be used to distinguish the target from surrounding objects. Moreover, the Frequency Response Method can detect very short distances since there is no minimum resolvable distance for this method.

❑ A comment on frequency response method

As we know, in practice, the step frequency range is limited within a bandwidth from $-\Delta f$ to Δf. Thus, the Fourier transform of the reflection coefficient consists of several *sinc* functions. The positions of the main lobes of the *sinc* functions indicate the locations of the discontinuities. The width of the main lobes decreases with increasing frequency range. If the distance between two discontinuities is less than half the extension of a main lobe, the two discontinuities can no longer be measured separately. The smallest distance of separation of discontinuities is

$$x_{min} = \frac{c}{4\Delta f} \tag{2.32}$$

For distance measurement, this limits the ability in distinguishing the near surrounding objects. If the surrounding object is too close to the target, the Frequency Response Method can not distinguish the target from surrounding object. The nearest distance that can be separated depends on the bandwidth of the transmitted signal.

2.2.2.3 Direct phase measurement method

As we know, the complex reflection coefficient can be expressed as $\Gamma = \rho \exp(-j2kR)$, where ρ is the magnitude, R is the measured distance, and $k = 2\pi f/c$ is the propagation constant. When the frequency is swept across some bandwidth, the argument of complex reflection coefficient $\phi = 2kR$ is linearly proportional to frequency as shown in Fig. 2.10[14].

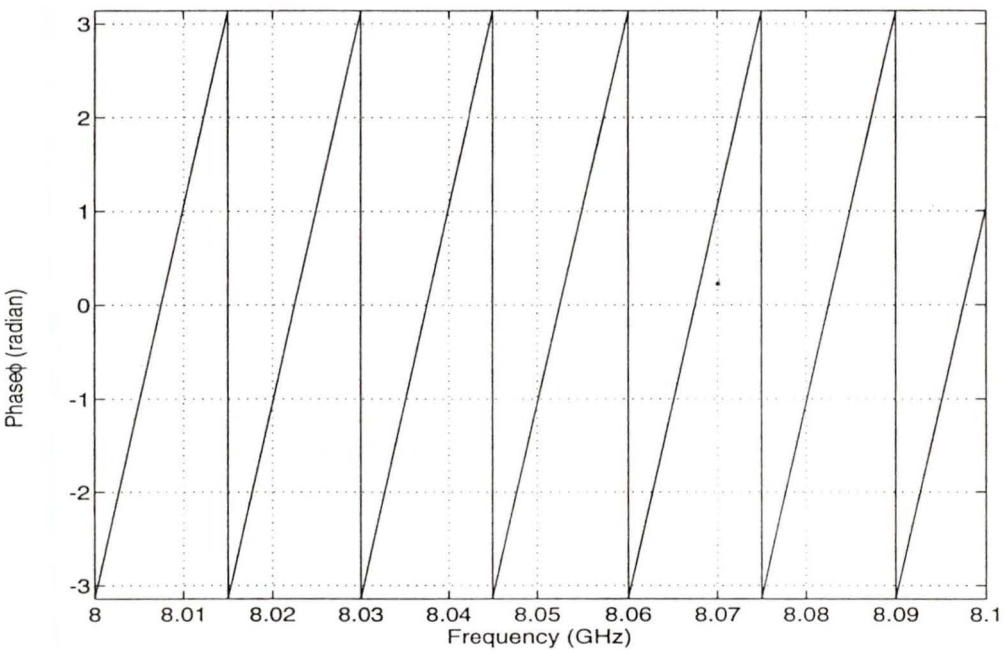

Figure 2.10 Argument of complex reflection coefficient vs. frequency

If the frequency is swept from f_{start} to f_{stop}, every null in the argument of the reflection coefficient represents 2π radians. Therefore, by counting the number of the nulls and comparing the phase difference between f_{stop} and f_{start}, we can obtain the distance R as follow

$$R = \frac{c\,(2\pi N + \Delta\phi)}{4\pi\Delta f} \tag{2.33}$$

or

$$R = \frac{c\,[2\pi\,(N-1) + \Delta\phi]}{4\pi\Delta f} \tag{2.34}$$

where N is the number of nulls, and $\Delta\phi$ is the phase difference between f_{stop} and $f_{start.}$ i.e $\Delta\phi = \phi(f_{stop}) - \phi(f_{start})$, $\Delta f = f_{stop} - f_{start}$

If $\Delta\phi > 0$, (2.33) is used, otherwise, the solution is (2.34). Direct phase measurement method measures the total phase of the argument of the reflection coefficient while the frequency is stepping. So, it has no ambiguous range and the measurable distance is extended.

2.2.2.4 Computer controlled stepped frequency reflectometry

Stepped frequency reflectometry employs the frequency-domain reflectometry technique to calculate the relative distance. The principle behind this method is the formation of a power standing wave pattern caused by the superposition of the transmitted and reflected wave [14]. It will be shown later that this power standing wave pattern can be represented by a pure sinusoid.

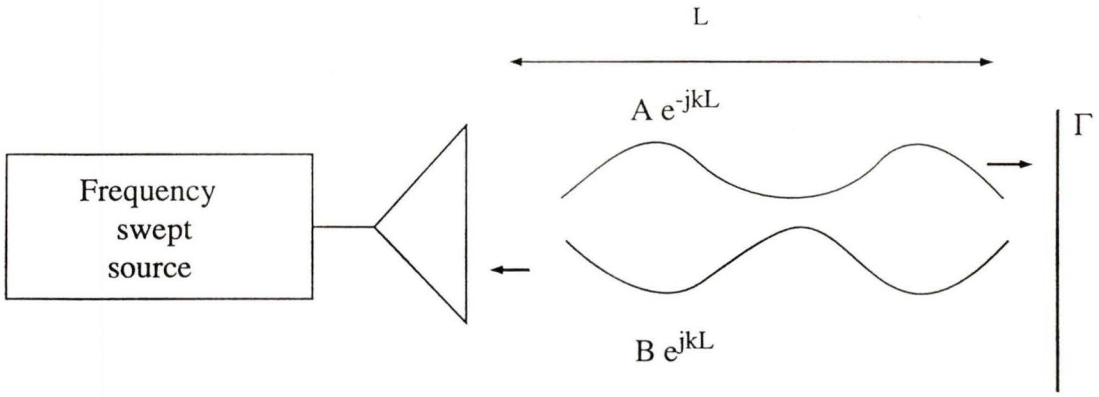

Figure 2.11 Formation of standing wave [14]

As shown in Fig. 2.11, the transmitted signal is $A\exp(-jkR)$ and the received reflected signal is $B\exp(jkR)$, where A and B are considered constant, R is the distance

between the transmitter and target, and $k = 2\pi f/c$ is the propagation constant. If a "square law" device is used to detect the power of the standing wave caused by the superposition of transmitted and reflected signals, the output of the "square law" device P_{out} is

$$\begin{aligned} P_{out} &= |A\exp(-jkR) + B\exp(jkR))|^2 \\ &= A|\exp(-jkR) + \rho\exp(jkR)|^2 \\ &= A|1 + \rho\exp(j2kR)|^2 \\ &= A|1 + \rho\cos(2kR) + j\rho\sin(2kR)|^2 \\ &= A + AB + 2B\cos(2kR) \end{aligned} \tag{2.35}$$

The P_{out} consists of two components, one is a DC component $A+AB$, the other is a standing wave component $2B\cos(2kR)$. When a balanced mixer is used, the DC component can be ignored. So, we can see that this power standing wave is a pure sinusoidal function of frequency as shown in Fig. 2.12.

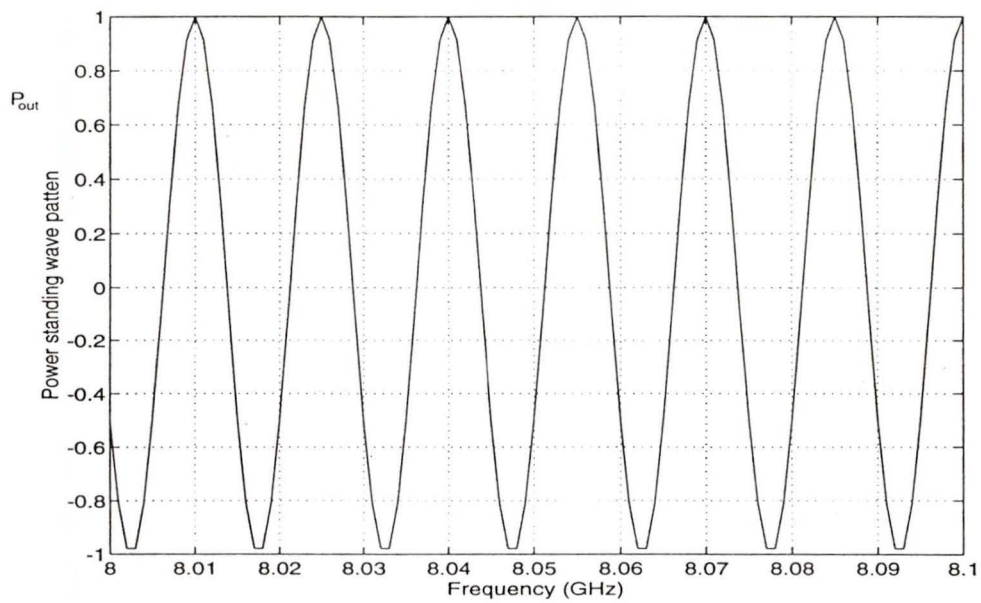

Figure 2.12 Power standing wave pattern

The principle and analysis of the Stepped Frequency Reflectometry is implemented by stepping the frequency from a start frequency f_{start} to a stop frequency f_{stop}, and determining the number of maxima N of the standing signal across the stepped bandwidth Δf. Since $P_{out} = 2B\cos(4\pi fR/c)$, the number of maxima N is

$$N = \frac{2(f_{stop} - f_{start})R}{c} \tag{2.36}$$

So, the distance R

$$R = \frac{cN}{2\Delta f} \tag{2.37}$$

To determine N, we sample the P_{out} and apply an FFT to the sampled data. The position of delta function in the transformed domain is equal to N. Thus, using (2.37), we obtain the distances.

The minimum resolvable distance δR is determined when exactly one maxima occurs across the stepped bandwidth Δf. As the bandwidth is increased, the resolvability of the distance increase.

$$\delta R = \frac{c}{2\Delta f} \tag{2.38}$$

However, for a fixed number of samples, a larger bandwidth decreases the maximum possible distance that can be measured, since as the number of the maxima approaches the sample length, cause the FFT to fail. For example, if we chose the number of sample as M, the sample interval is $f_s = \Delta f/M$. Since $P_{out} = \cos(4\pi fR/c)$, according to Nyquist's criterion, f_s should be smaller than $c/4\pi R$, that is $\Delta f/M \leq c/4\pi R$. So, for a given number of samples, the maximum measurable distance is

$$R_{max} = \frac{cM}{4\pi\Delta f} \tag{2.39}$$

2.2.2.5 Computer controlled direct timing technique

From the above discussion, we conclude that the power standing wave pattern is represented by a pure sinusoid, $P_{out} = P\cos(2kR)$. Since $k = 2\pi f/c$ and f is a function of time (i.e., stepped from f_{start} to f_{stop} in duration time), k is also a function of time [14]. For simplicity, let's assume $f = f_{start} + (f_{stop} - f_{start})t/T$, where T is the swept duration time. So, k is

$$k = \frac{2\pi\Delta f}{cT}t \tag{2.40}$$

where Δf is $f_{stop} - f_{start}$

Thus, the P_{out} is also a sinusoidal function of time as shown in Fig. 2.13.

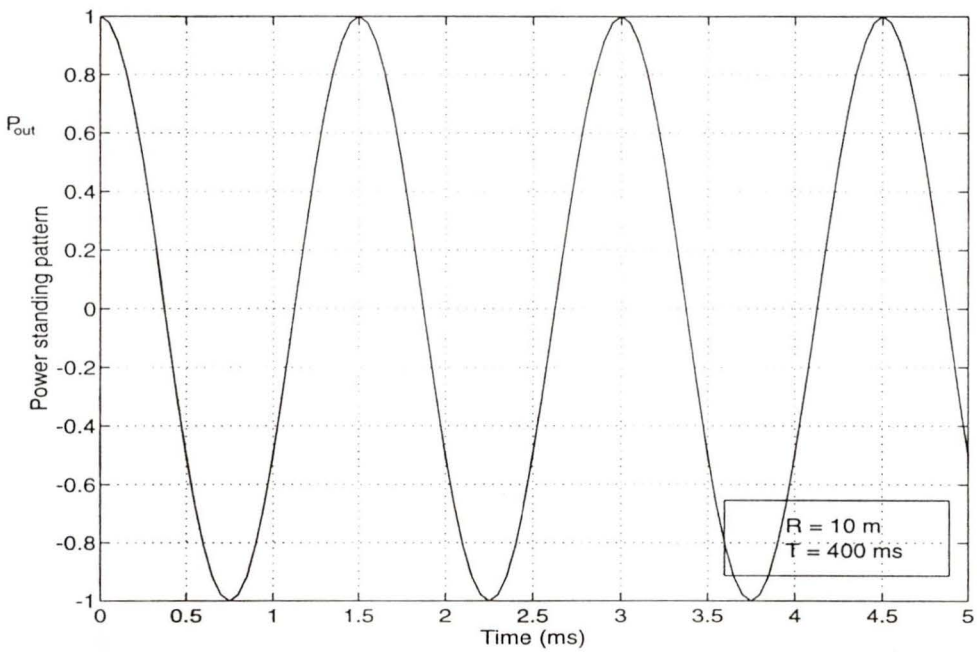

Figure 2.13 Output power versus time.

Let τ be the period of the standing wave pattern, since $P_{out} = P\cos(4\pi\Delta fR/cT)$, we can obtain

$$\tau = \frac{cT}{2\Delta fR} \tag{2.41}$$

So, the distance R

$$R = \frac{cT/\tau}{2\Delta f} \tag{2.42}$$

By measuring the period of the standing wave pattern, we obtain the distance.

In fact, the direct timing method uses the same principle as that in the stepped frequency reflectometry. It effectively determines the number N in (2.37) more accurately and directly in the time domain. Thus, it does not require a complicated signal processing unit as that in the stepped frequency reflectometry and has higher accuracy. Moreover, it is easy to manufacture and kept within a small physical volume and can be made portable.

Chapter 3

Surface waveguides

A surface waveguide is an open boundary structure capable of supporting modes which are intimately bound to the surface of the structure. The field is characterized by an exponential decay away from the surface and have the usual propagation function $\exp(-j\beta z)$ along the axis of the structure [15]. In this chapter, two kinds of surface waveguides, the dielectric rod and Goubau line, are introduced. The description of the parameters which are important for the design of the transmission medium for MLGS, including propagation velocity, field confinement and transmission losses are presented. The chapter is closed with a brief comparison between these two kinds of surface waveguides and some other transmission structures.

3.1 Dielectric rod waveguide

3.1.1 General principles

The structure of the dielectric rod waveguide is illustrated in Fig. 3.1 [16]. The rod material is assumed to be a perfect dielectric characterized by the real scalar permittivity $\varepsilon = \varepsilon_0\varepsilon_r$ and the real scalar permeability μ_0.

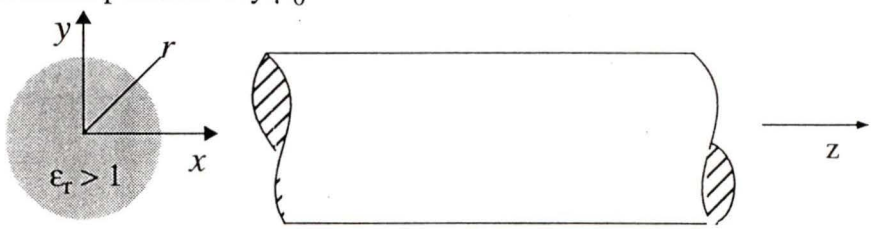

Figure 3.1 Dielectric rod waveguide

Inside the rod, E_z and H_z are finite at the origin, and periodic with a period of 2π with respect to ϕ. Furthermore, they represent waves traveling in the positive z direction. These requirements can be met by choosing E_z and H_z in the form:

$$E_{z1} = AJ_m(k_{\rho 1}\rho)\cos(m\phi)\, e^{-j\beta z} \tag{3.1}$$

$$H_{z1} = BJ_m(k_{\rho 1}\rho)\sin(m\phi)\, e^{-j\beta z} \tag{3.2}$$

where J_m is the Bessel function of the first kind and mth order, and

$$k_{\rho 1}^2 = k^2 - \beta^2 = k_0^2\varepsilon_r - \beta^2 \tag{3.3}$$

where k_0 is the wave number in free space.

Outside the rod, E_z and H_z are similarly periodic with a period of 2π with respect to ϕ, and represent traveling waves along the z-axis. However, unlike the components inside the rod, they are decaying exponentially in the radial direction and therefore the wave is guided along the rod. Thus,

$$E_{z2} = CK_m(k_{\rho 2}\rho)\cos(m\phi)\, e^{-j\beta z} \tag{3.4}$$

$$H_{z2} = DK_m(k_{\rho 2}\rho)\sin(m\phi)\, e^{-j\beta z} \tag{3.5}$$

where K_m is the modified Bessel function of the second kind and mth order, and

$$k_{\rho 2}^2 = \beta^2 - k_0^2 \tag{3.6}$$

where A, B, C, D are amplitudes of the field and to be determined from boundary conditions.

The transverse field components inside and outside the rod are

❑ Inside the rod

$$
\begin{aligned}
E_{\rho 1} &= \frac{1}{k_{\rho 1}^2}\left[-j\beta k_{\rho 1} A J_m'(k_{\rho 1}\rho) - j\omega\mu_0 m\frac{B}{\rho} J_m(k_{\rho 1}\rho)\right]\cos(m\phi)\, e^{-j\beta z} \\
E_{\phi 1} &= \frac{1}{k_{\rho 1}^2}\left[j\beta m\frac{A}{\rho} J_m(k_{\rho 1}\rho) + j\omega\mu_0 k_{\rho 1} B J_m'(k_{\rho 1}\rho)\right]\sin(m\phi)\, e^{-j\beta z} \\
H_{\rho 1} &= \frac{1}{k_{\rho 1}^2}\left[-j\beta k_{\rho 1} B J_m'(k_{\rho 1}\rho) - j\omega\varepsilon m\frac{A}{\rho} J_m(k_{\rho 1}\rho)\right]\sin(m\phi)\, e^{-j\beta z} \\
H_{\phi 1} &= \frac{1}{k_{\rho 1}^2}\left[-j\beta m\frac{B}{\rho} J_m(k_{\rho 1}\rho) - j\omega\varepsilon k_{\rho 1} A J_m'(k_{\rho 1}\rho)\right]\cos(m\phi)\, e^{-j\beta z}
\end{aligned}
\tag{3.7}
$$

❑ Outside the rod

$$
\begin{aligned}
E_{\rho 2} &= \frac{-1}{k_{\rho 2}^2}\left[-j\beta k_{\rho 2} C K_m'(k_{\rho 2}\rho) - j\omega\mu_0 m\frac{D}{\rho} D_m(k_{\rho 2}\rho)\right]\cos(m\phi)\, e^{-j\beta z} \\
E_{\phi 2} &= \frac{-1}{k_{\rho 2}^2}\left[j\beta m\frac{C}{\rho} J_m(k_{\rho 2}\rho) + j\omega\mu_0 k_{\rho 1} B K_m'(k_{\rho 2}\rho)\right]\sin(m\phi)\, e^{-j\beta z} \\
H_{\rho 2} &= \frac{1}{k_{\rho 2}^2}\left[-j\beta k_{\rho 2} D K_m'(k_{\rho 2}\rho) - j\omega\varepsilon m\frac{C}{\rho} K_m(k_{\rho 2}\rho)\right]\sin(m\phi)\, e^{-j\beta z} \\
H_{\phi 2} &= \frac{1}{k_{\rho 2}^2}\left[j\beta m\frac{D}{\rho} K_m(k_{\rho 2}\rho) + j\omega\varepsilon_0 k_{\rho 2} C K_m'(k_{\rho 2}\rho)\right]\cos(m\phi)\, e^{-j\beta z}
\end{aligned}
\tag{3.8}
$$

The TM and TE modes are possible if the fields are independent of the angular coordinates. Otherwise, six field components are present and the propagation mode is a hybrid of TE and TM, i.e HE or EH modes.

Applying boundary conditions to the field components inside and outside the rod, we get following equations:

$$F_1(x)F_2(x) - F_3^2(x) = 0 \tag{3.9}$$

where

$$F_1(x) = \frac{J'_m(x)}{x} + \frac{K'_m(y)\,J_m(x)}{\varepsilon_r y K_m(y)} \tag{3.10}$$

$$F_2(x) = \frac{J'_m(x)}{x} + \frac{K'_m(y)\,J_m(x)}{y K_m(y)} \tag{3.11}$$

$$F_3(x) = \frac{\beta a m}{k_0 a \sqrt{\varepsilon_r}} J_m(x)\left(\frac{1}{x^2} + \frac{1}{y^2}\right) \tag{3.12}$$

$$x = k_{\rho 1} a \tag{3.13}$$

$$y = k_{\rho 2} a = \sqrt{(k_0 a)^2 (\varepsilon_r - 1) - x^2} \tag{3.14}$$

Equation (3.9) is called the eigenvalue equation, the solutions of which are called the eigenvalues of the dielectric rod waveguide. The eigenvalue x is a measure of the steepness of the field gradient in the radial direction. The relation between eigenvalue x and propagation constant β is

$$\beta a = \sqrt{(k_0 a)^2 \varepsilon_r - x^2} \tag{3.15}$$

The eigenvalues can be determined by solving the transcendental eigenequation (3.9). The evaluation of eigenvalues has to be carried out numerically. Figure 3.2 shows the eigenvalues of HE_{11} mode for several different rods.

Figure 3.3 illustrates the ratio of the guided wavelength to that in the free space. The guided wavelength falls between the free space wavelength and the wavelength when all the space is filled with the dielectric material.

The cutoff condition for the dielectric waveguide is $k_0 = \beta$. Substituting k_0 by β in eigenequation, we get the cutoff eigenvalue x_c which determines the cutoff frequency of each propagation mode. The cutoff frequency f_c can be written as

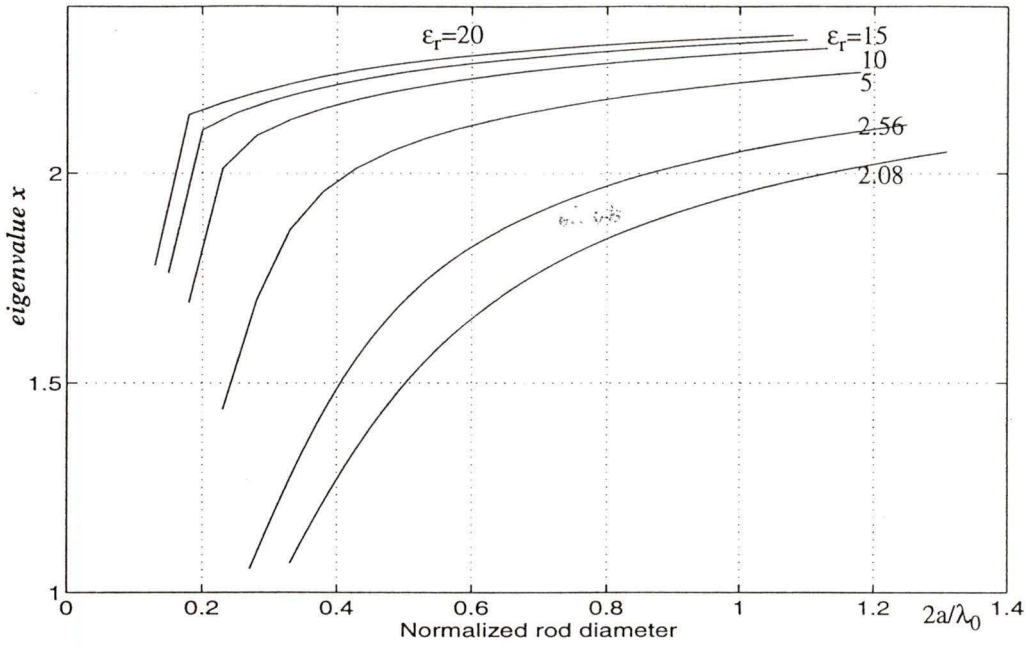

Figure 3.2 The eigenvalues of the HE_{11} mode for several kinds of rods

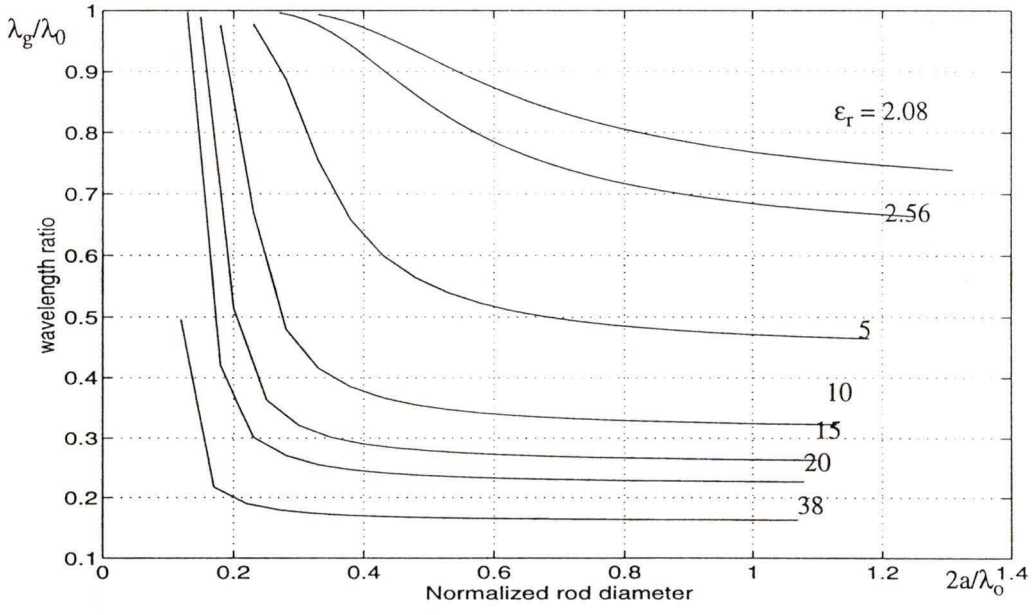

Figure 3.3 Phase ratio λ_g/λ_o of surface waveguide

$$f_c = \frac{x_c c}{2\pi a\sqrt{\varepsilon_r - 1}} \tag{3.16}$$

where x_c is the cutoff eigenvalue.

The cutoff eigenvalues of several modes are as follows:

† HE_{11} mode -- $x_c = 0$

† TM_{01} and TE_{01} mode -- $x_c = 2.405$

† HE_{13} mode -- $x_c = 3.832$

† HE_{15} mode -- $x_c = 7.016$

So, the HE_{11} mode is the dominant mode and has no cutoff frequency. The single mode propagation condition is

$$0 < \frac{2a}{\lambda_c} < \frac{2.405}{\pi\sqrt{\varepsilon_r - 1}} \tag{3.17}$$

In addition, from (3.8), we can see that $y=k_{\rho 2}a$ should be real. If the material outside the dielectric rod is not air but something with higher dielectric constant than that of the rod, that is $\varepsilon_{out} > \varepsilon_{rod}$, y becomes purely imaginary. In this case, the fields outside rod are no longer described by modified Bessel functions K_m but Hankel functions $H_m^{(2)}$ representing outwardly travelling wave.

3.1.2 Field confinement

Since for surface waveguides, waves propagate both inside and outside the structure, the physical dimension of the structure no longer represents the field extension in radial direction. An important characterization of surface waveguides is the field confinement. Usually, this characterization is described by two terms: (1) power ratio; and (2) effective diameter.

For the dielectric rod, the power ratio is the ratio of the total power transmitted outside rod to the total transmitted power, which gives a measure of field containment in the

rod. We know the field expressions of dielectric rod, so we can obtain the power ratio easily. It can be expressed as:

$$\frac{P_{out}}{P} = \frac{P_{out}}{P_{in} + P_{out}} = \frac{1}{1 + P_{in}/P_{out}} \tag{3.18}$$

where P_{in}, P_{out} are the power inside and outside rod and

$$\frac{P_{out}}{P_{in}} = \frac{x^2\left(\frac{1}{\varepsilon_r} + R\right)V}{y^2(1+R)U} \times \frac{1+D_2}{1+D_1} \tag{3.19}$$

where

$$R = \frac{F_1(x)}{F_2(x)}$$

$$U = \frac{J_m^2(x)}{J_m(x)} + \frac{2J_m(x)}{xJ_m(x)} + \left(1 - \frac{m^2}{x^2}\right)$$

$$V = \frac{K_m(y)}{K_m^2(y)} - \frac{2K_m(y)}{yK_m(y)} + \left(1 + \frac{m^2}{y^2}\right)$$

$$D_1 = -\frac{2mk_0\sqrt{\varepsilon_r}R\left(1 + \beta^2/k_0^2\varepsilon_r\right)}{\beta x^2(1+R)U}$$

$$D_2 = \frac{2mk_0\sqrt{\varepsilon_r}R\left(1 + \beta^2/k_0^2\right)}{\beta y^2(1+\varepsilon_r R)V}$$

and Fig. 3.4 shows the power ratios of several rods. From Fig. 3.4 we can see that with the increase of the dielectric constant, more and more energy is transmitted inside the rod.

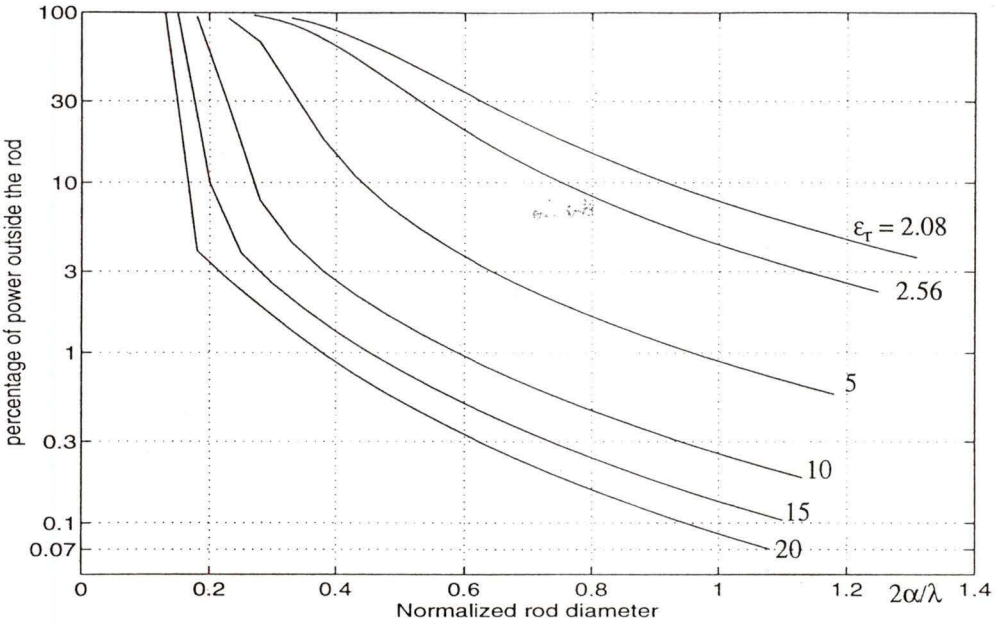

Figure 3.4 Power ratio of several rods

The effective diameter is defined as twice the radius at which the axial field density has decreased by 20 dB. This larger value was chosen in preference to the e^{-1} decrease since it places less burden on precise measurement of small attenuation. By (3.4), we can get the expression of the effective diameter d_{eff} as

$$10log\left(\frac{E_z(d_{eff}/2)}{E_z(a)}\right)^2 = -20$$

$$so \qquad 20log\left(\frac{K_1(k_{\rho 2}d_{eff}/2)}{K_1(y)}\right) = -20 \tag{3.20}$$

Figure 3.5 shows the ratio of effective diameter to the physical diameter for several rods. The effective diameters decrease with the increasing of the rod dielectric constant. This is very consistent with previous discussion that for higher dielectric constant rod, more energy is transmitted inside the rod and thus d_{eff} is smaller.

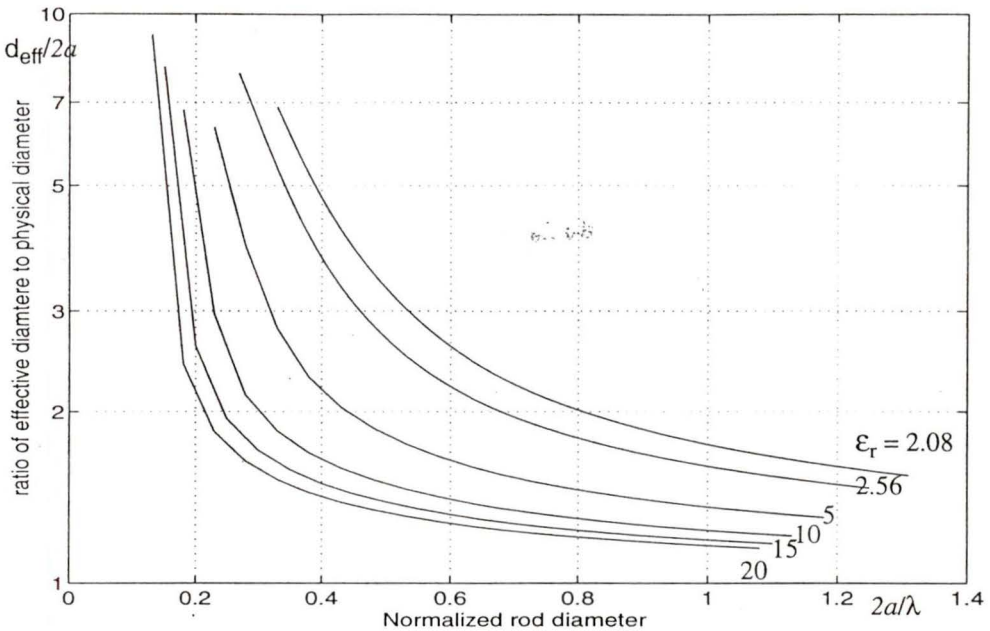

Figure 3.5 The effective diameter of the several kinds of dielectric rods

3.1.3 Attenuation of dielectric rod waveguide

Losses of the dielectric rod waveguide occur due to three principal causes: There are in general radiation and reflection losses at transitions caused by imperfect matching; there is radiative loss if the rod is curved; finally, there is the dielectric loss in the material of the rod if the latter is not a perfect dielectric [18]. The third loss is the main loss for dielectric rod waveguide.

Assuming the complex dielectric constant of the material is $\varepsilon_r = \varepsilon' - j\varepsilon''$. The loss can be calculated by a perturbation method and can be expressed as [18]

$$\alpha = 2729\,(\varepsilon' \tan\delta / \lambda_0)\, R \qquad dB/m \qquad (3.21)$$

where λ_0 is the free space wavelength and in the unit cm, $\tan\delta$ is the loss tangent of the rod material, R is the attenuation factor, and for the dominant mode (HE_{11} mode), if the y is very small and the eigenvalue x is not too large, R can be expressed approximately as

$$R = y^2\left[4/x^4 + (\varepsilon' - 1)/4x^4 - \frac{(\varepsilon' + 1)}{32}\right]$$

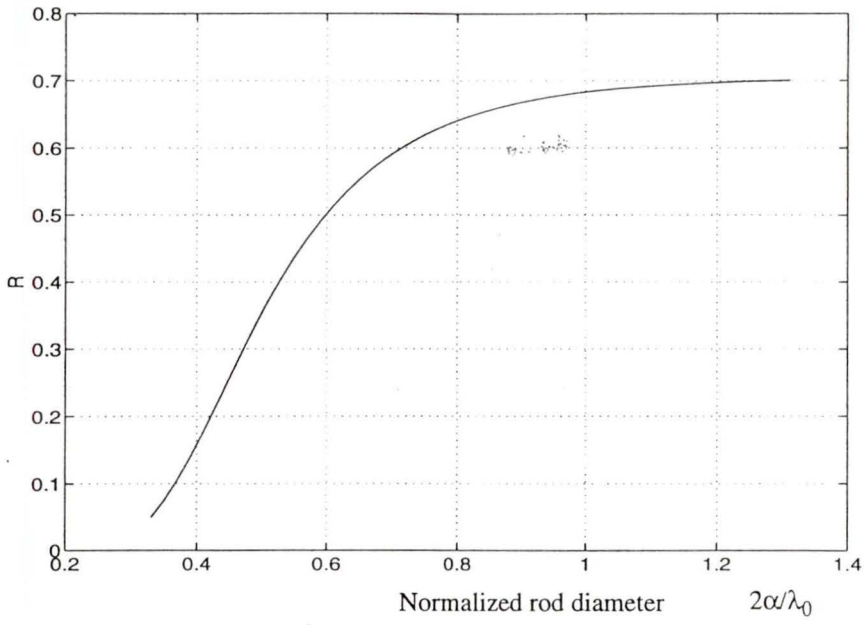

Figure 3.6 Attenuation factor R vs. normalized diameter $2a/\lambda$

Figure 3.6 shows the attenuation factor R versus the normalized rod diameter $2a/\lambda$ for a teflon rod. As $2a/\lambda$ increases beyond the cutoff value, R converges toward the value $1/(\varepsilon_r)^{1/2} = 0.694$ which is the attenuation factor for a plane wave in an infinite medium.

Figure 3.7 shows the attenuation versus frequency for 3/8" diameter teflon rod. The attenuation increases with the increase of rod dimension and operation frequency. This is because more energy is inside the rod when it has a larger diameter or is operated at higher frequency. The selections of the diameter of the rod and the operation frequency are a comprise between attenuation and field confinement.

Figure 3.7 Attenuation of teflon rod

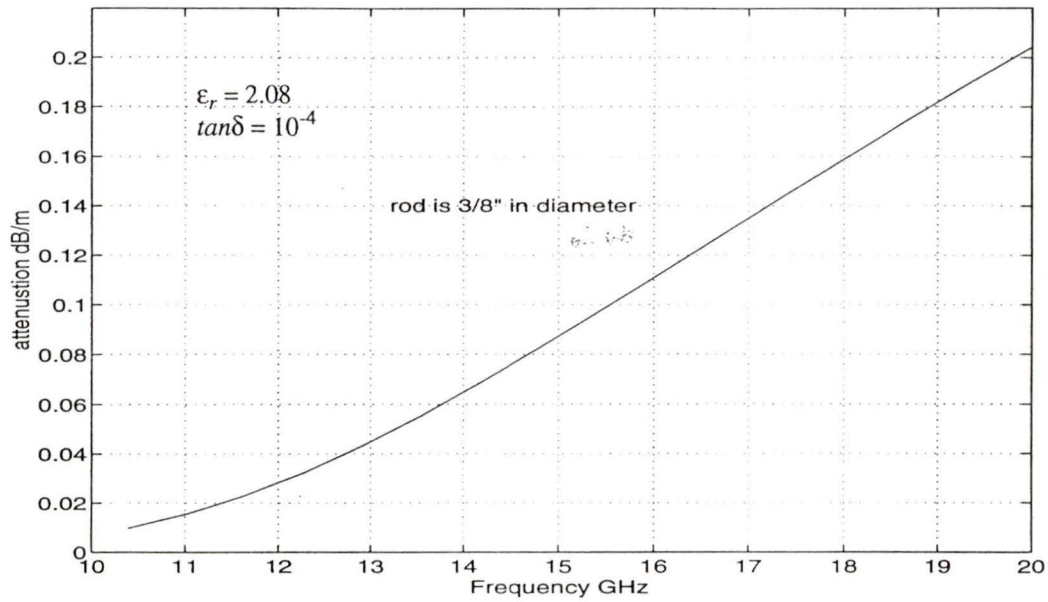

3.1.4 Dielectric Image Line

The HE_{11} mode in the dielectric rod waveguide is an asymmetric, hybrid mode which has components of both electric and magnetic field in the direction of propagation. The electric field lines in the HE_{11} mode in the dielectric rod waveguide is shown in Fig. 3.8. From Fig. 3.8 we can see that the transverse field distribution of the HE_{11} mode is such that a metal sheet may be passed through the axis of the rod without disturbing the field. A half-round rod mounted on a metal ground plane is the dielectric image line [19], as shown in Fig. 3.9.

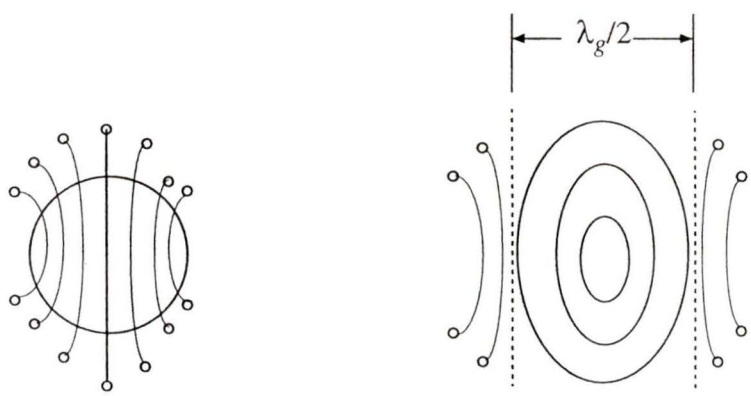

Figure 3.8 E field of dielectric rod waveguide (HE_{11} mode)

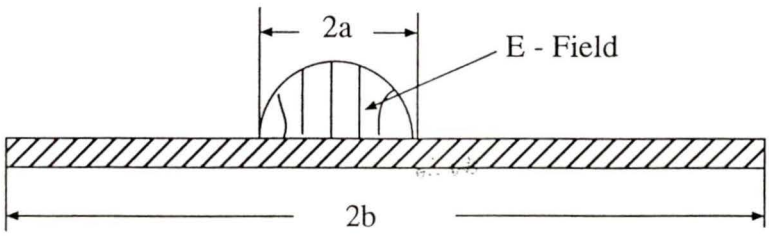

Figure 3.9 Dielectric Image Line

The extension of the field is determined by the ratio of diameter of the conductor plane to the wavelength. The line loss for a half round dielectric rod on an infinite image surface is composed of the dielectric loss and the conductor loss which is due to the finite conductivity of the image plane. This has been studied in detail and an analytical expression has been given in [20]. The dielectric loss and conductor loss for a teflon-copper image line are shown in Fig. 3.10. The rod is 3/8" in diameter. We can see that the dielectric loss is much larger than the conductor loss.

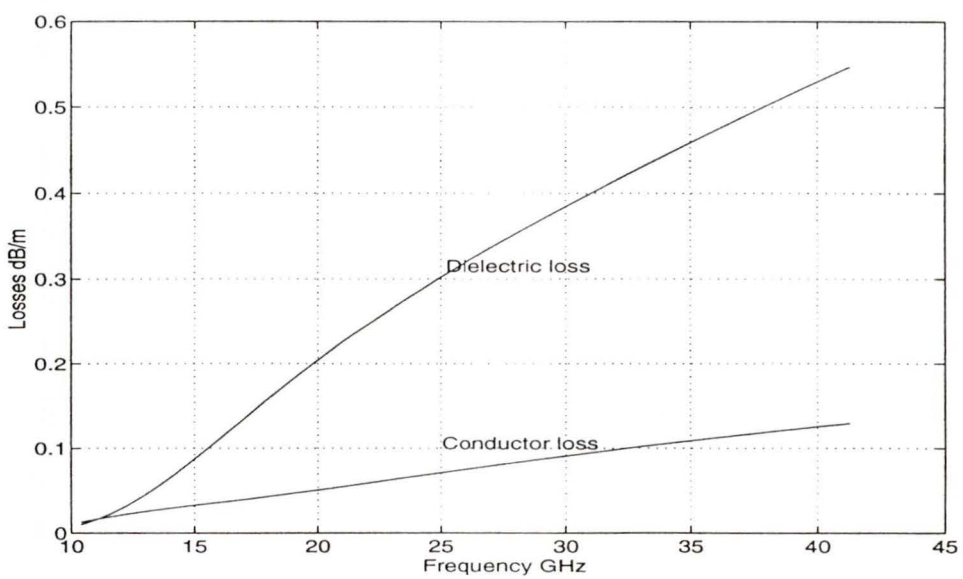

Figure 3.10 Attenuation of dielectric image line

The advantages of the dielectric image line may be summarized as follows:

1. No mechanical support is required,
2. coupling from the rear through slots is feasible,
3. the field extension is positively indicated by the width of the image plane,
4. minimal attenuation at millimeter wavelengths is afforded by choosing a large image screen and a thin dielectric filament,
5. construction is simple.

3.2 Goubau Line

3.2.1 General principles

In 1899, A. Sommerfeld published a paper about surface waves propagating along a single conductor line of finite conductivity. Although the theoretical transmission losses for such a wave is very low, experiments showed that the field in such a line is the same as that in an antenna made of a perfect conductor. More precise experiments showed that the Sommerfeld's wave did exist but it was too weak to be observed. The reason for this is that the usual coupling devices excite mainly the radiating wave while Sommerfeld's wave requires launching devices of very large dimension. Moreover, the large field extension, which requires large clearance around the conductor to avoid severe distortion of the field, also makes it impractical.

It is of interest that the usual imperfection of the surface of a conductor can be sufficient to convert Sommerfeld's wave into another wave mode, a wave mode which is mainly determined by the surface condition. This type of wave is of particular interest since the extension of the field can be controlled by the modification of the conductor surface. One such surface modified transmission line was studied by G. Goubau (Goubau line) [21]. and Figure 3.11 shows the structure of it [22].

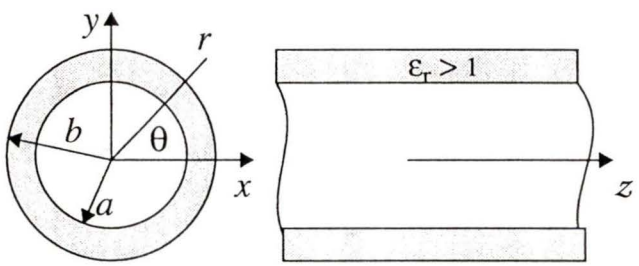

Figure 3.11 Dielectric-coated-wire surface waveguide (Goubau line)

The Goubau line consists of a conductor coated with a dielectric layer. The wave mode is a radially-symmetrical transverse magnetic field and propagates in two regions: within the dielectric layer and outside the line. In the dielectric region, the wave propa-

gates in the z direction with propagation factor $exp(-j\beta z)$ and can be described by Bessel functions (J_0, J_1, Y_0, Y_1). Outside the line, the wave propagates in z direction and decays in the radial direction with factor $K_0(hr)$, where K_0 is the modified Bessel function of zeroth order. The field components can be written as [22].

❑ Field inside the dielectric layer

$$e_z = C_1 J_0(k_d r) + C_2 Y_0(k_d r) \qquad a < r < b \tag{3.22}$$

❑ Field outside the line

$$e_z = C_3 K_0(hr) \qquad r > b \tag{3.23}$$

The transverse electric field is given by

$$e_t = -\frac{j\beta}{k_c^2} \nabla_t e_z \tag{3.24}$$

where $k_c = k_d$ in the dielectric region and $k_c = jh$ in the surrounding air region

Applying boundary conditions to (3.22) - (3.24), we obtain following relations

$$C_2 = -C_1 \frac{J_0(k_d a)}{Y_0(k_d a)} \tag{3.25}$$

$$C_3 K_0(hb) = C_1 \left[J_0(k_d b) - \frac{Y_0(k_d b)\, J_0(k_d a)}{Y_0(k_d a)} \right] \tag{3.26}$$

$$\beta^2 = \varepsilon_r k_0^2 - k_d^2 = k_0^2 + h^2 \tag{3.27}$$

and the eigenvalue equation

$$\frac{k_d K'_0(hb)}{K_0(hb)} = -\varepsilon_r h \frac{J'_0(k_d b)\, Y_0(k_d a) - Y'_0(k_d b)\, J_0(k_d a)}{J_0(k_d b)\, Y_0(k_d a) - J_0(k_d a)\, Y_0(k_d b)} \tag{3.28}$$

This transcendental equation must be solved simultaneously with (3.27) in order to

determine h, which is called the eigenvalue of the Goubau line. Numerical methods which were employed for the dielectric rod problem may be used. However, for the case when the dielectric layer is thin compared with the wire radius, or the layer is of the same order of magnitude as the wire radius, but the radius itself is very small compared with the wavelength, the transcendental equation can be simplified as follows

$$ln\frac{b}{a} = -\varepsilon_r \frac{h^2}{k_d^2} ln 0.89hb \tag{3.29}$$

The relation between wire diameter, dielectric layer and phase velocity reduction is shown in Fig. 3.12.

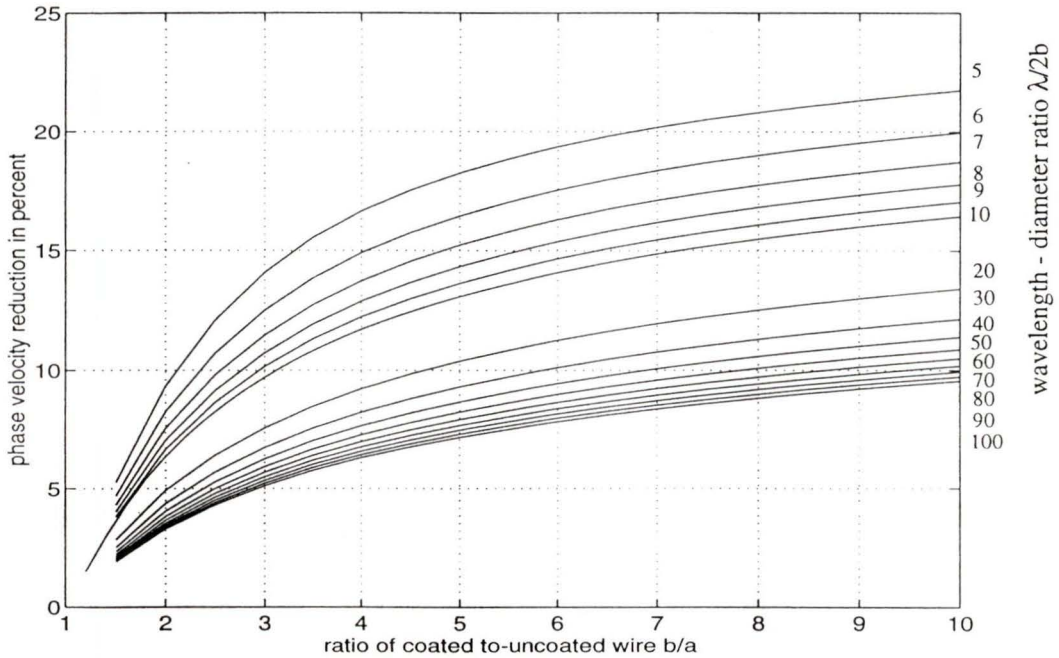

Figure 3.12 Relationships between wire diameter, dielectric layer and phase velocity

3.2.2 Field confinement

Usually, the dielectric layer of the Goubau line is very thin and the energy within the layer can be negligible. The field confinement is described by a parameter ρ_p which is the radius of a circle within which a certain percentage p of the total power of the surface wave travels and it is given by the equation [21]:

$$p = 1 - \frac{F(h\rho_p)}{F(hb)} \tag{3.30}$$

where h is the eigenvalue, b is the outer radius of the line and F can be expressed as

$$\frac{F(h\rho_p)}{(h\rho_p)^2} = -\frac{2}{h\rho_p} jH_1^{(1)}(jh\rho_p) H_1^{(1)}(jh\rho_p) - \left[H_0^{(1)}(jh\rho_p)\right]^2 - \left[H_1^{(1)}(jh\rho_p)\right]^2 \tag{3.31}$$

where H is the Hankel function

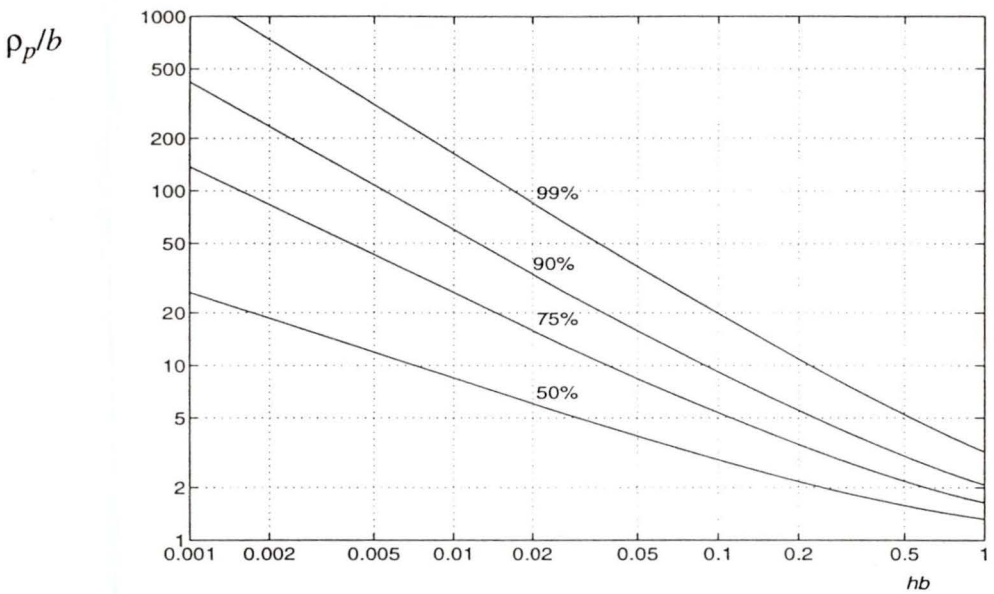

Figure 3.13 Percent of power within given radius at 10 GHz

Figure 3.13 shows the ratio ρ_p/b as a function of hb for p = 50 percent, 75 percent, 90 percent and 99 percent. For a given radius b of the guide, the field decreases faster with increasing h.

The effective diameter d_{eff}, which is defined in section 3.13, can also be used to describe the field extension of the line. From (3.23), we can get the expression of the effective diameter d_{eff} as follows:

$$10log\left(\frac{E_z\left(\frac{d_{eff}}{2}\right)}{E_z(a)}\right)^2 = -20$$

$$20log\left(\frac{K_0(hd_{eff}/2)}{K_0(hb)}\right) = -20 \tag{3.32}$$

and Fig. 3.14 illustrates the ratio of $d_{eff}/2b$ versus hb.

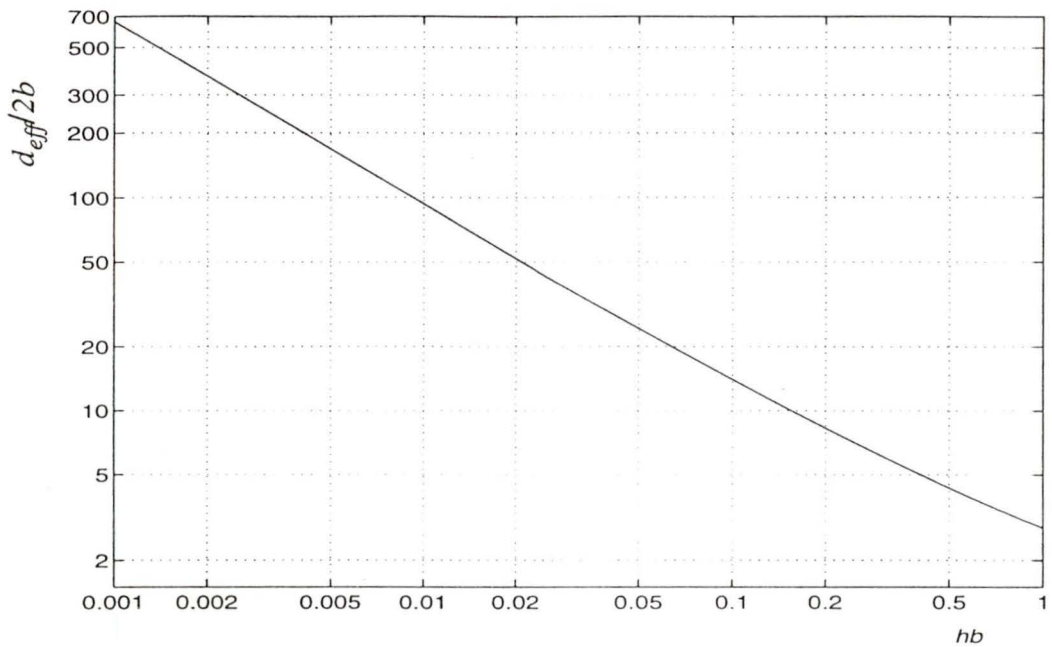

Figure 3.14 Effective diameter for various lines at 10 GHz

3.2.3 Attenuation

Losses for the Goubau line consist of two parts: conductor loss caused by the finite conductivity of the core and dielectric loss caused by the dielectric layer. These two losses can be calculated by a perturbation method and the final form can be written as [21]:

$$L_{c,\,100ft} = \frac{P(hb)}{a(\lambda_0)^{1/2}} \qquad (dB) \tag{3.33}$$

$$L_{i,\,100ft} = \frac{1}{\varepsilon_r - 1} tan\delta \frac{\lambda}{b^2} Q(hb) \qquad (dB) \tag{3.34}$$

with

$$P(hb) = -1.33 \times 10^{4} (\varepsilon_0/\mu_0)^{\frac{1}{4}} \left(\frac{\pi \mu_c}{\sigma_c \mu_0} \right)^{\frac{1}{2}} \frac{1}{lnhb + 0.38} \tag{3.35}$$

$$Q(hb) = 2.11 \times 10^{3} \left(1 - \frac{0.5}{lnhb + 0.38} \right) (hb)^{2} \tag{3.36}$$

where a and b are the radii of the core and the coated line

λ_0 is the free space wavelength

ε_0 and μ_0 are the permittivity and permeability of free space, respectively

ε_r and $tan\delta$ are the dielectric constant and loss factor of the dielectric layer, respectively

μ_c is the permeability of the core and σ_c is the conductivity

For a coated copper wire stretched in air,

$$P(hb) = \frac{-1.60}{lnhb + 0.38} \tag{3.37}$$

The function $P(hb)$ (for copper) and $Q(hb)$ are plotted in Fig. 3.15.

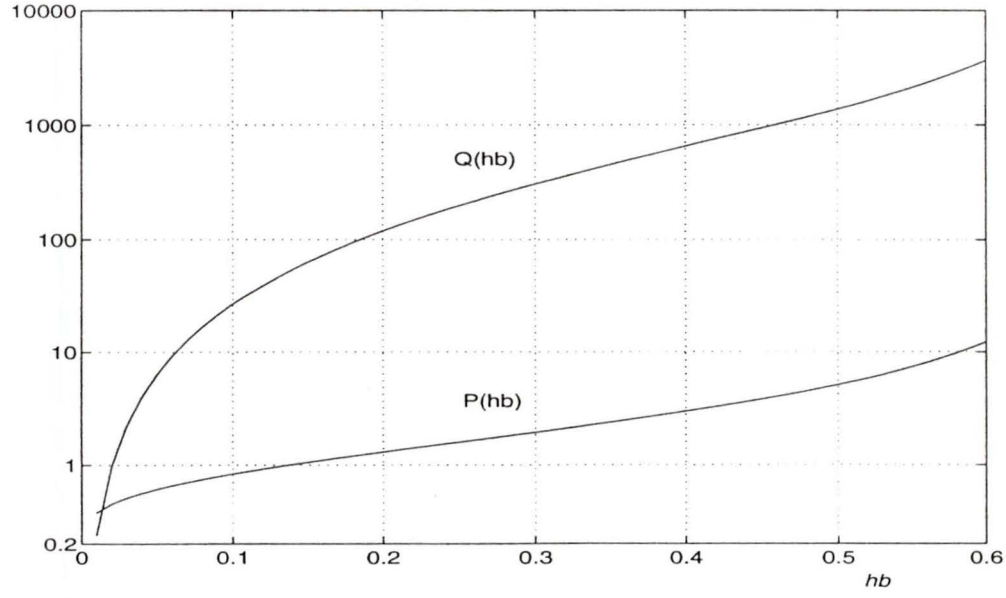

Figure 3.15 Chart for determining P and Q

The conductivity losses which are proportional to P change little with increasing layer thickness. The dielectric losses rises much faster. However, since only a small fraction of the energy propagates in the layer, the dielectric losses are usually small compared with the conductivity losses even for rather thick layers. Figure 3.16 shows the conductivity losses and dielectric losses versus frequency. The Goubau line is 10 mm in diameter and the dielectric layer is 1.5 mm.

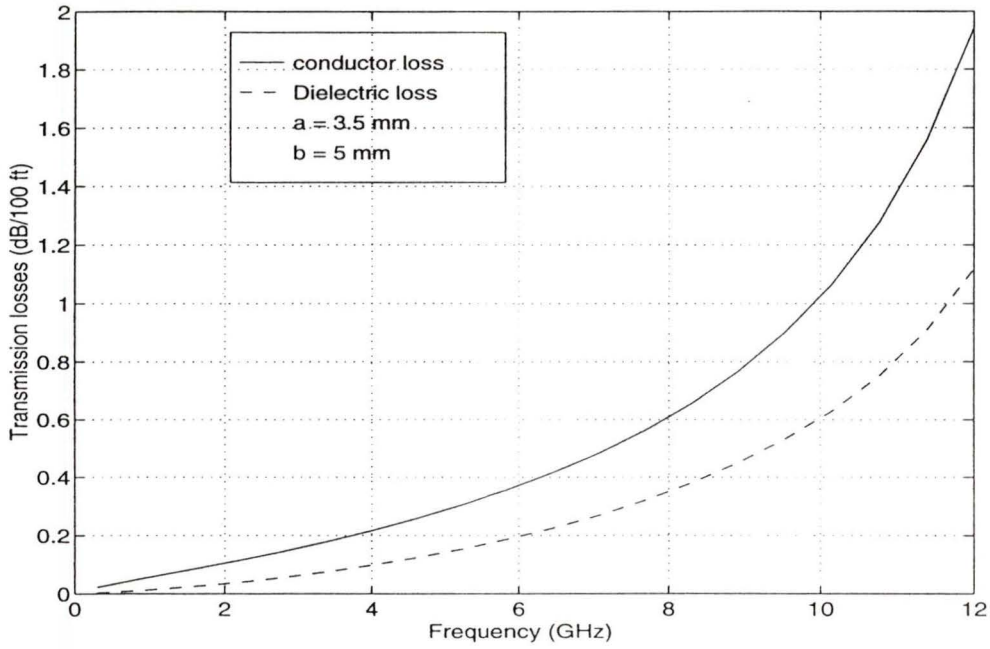

Figure 3.16 Conductor losses and dielectric losses of Goubau line

From the above discussion, we can generalize and make some statements about the losses of the Goubau line:

1. The losses of the Goubau line consist of the conductor losses and the dielectric losses caused by the imperfection of the conductor and dielectric material used.
2. Both losses rise with the increasing of the operation frequency.
3. Since there is no limitation on the diameter of the conductor as far as modes are concerned, the total losses can be made smaller by increasing the diameter of the conductor core.

However, in order to decrease the transmission losses, more energy has to propagate outside the line, this in turn increases the effective diameter of the line. Therefore, there is a trade-off between the transmission losses and the field confinement.

3.3 Excitation of Surface Waveguides

A factor of prime importance in all surface wave applications is the efficient excitation of the desired mode in the guide. The excitation efficiency of a source is defined as the ratio of the power converted to the surface wave mode to the total power which is delivered by the source. In order to excite the desired wave mode with high efficiency, a launching device is needed which develops within a cross section a field having a structure similar to that of surface wave [23]. For the dielectric rod, the mode which is often used is the HE_{11} mode and for the Goubau line it is the TM_{00} mode. Both of these are the lowest order modes which have no cutoff frequencies. Several investigators have shown that launching efficiencies of 80 percent or more can be obtained. Some commonly used methods of exciting surface waveguides are presented.

3.3.1 Dielectric rod waveguide

❑ Metal waveguide

This is one most generally used method of exciting dielectric waveguides. Since a rectangular metal guide operating in the dominant mode has an electric field whose configuration is roughly similar to then transverse component of the electric field in the HE_{11} mode of the dielectric guide, the transfer could be made simply by inserting the dielectric rod longitudinally into the metal guide for a short distance. Somewhat better transfer resulted when the rectangular metal guide carrying the TE_{10} mode was modified by a transition to circular guide, changing the mode to TE_{11} [25][26]. The dielectric rod, tapering from a point to minimize reflection, was inserted to fill the open end of the circular guide. A typical transition of this type is shown in Fig. 3.17(a).

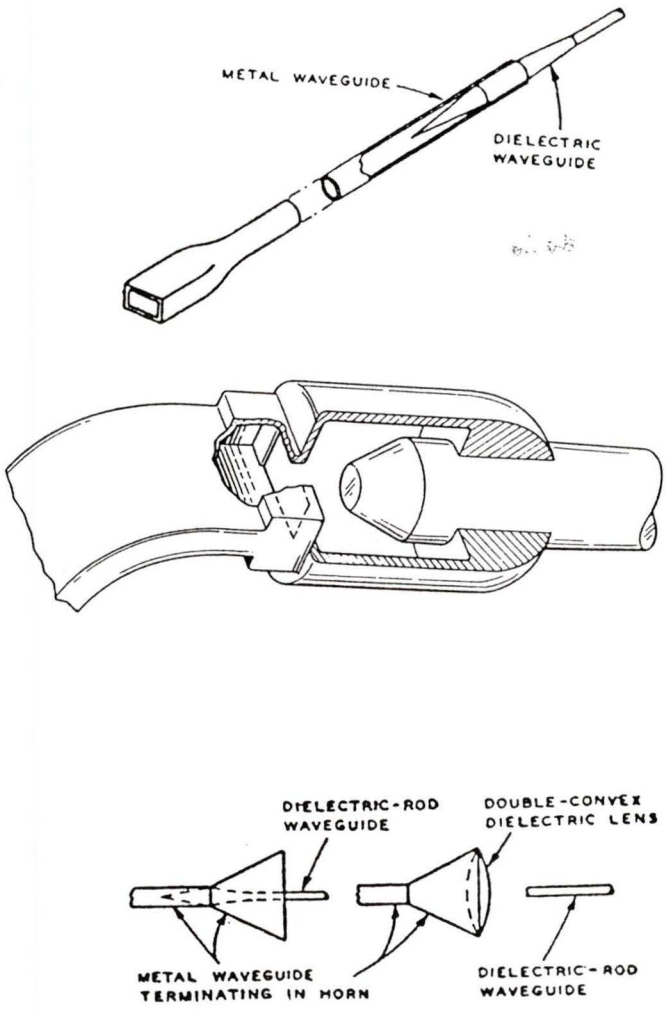

Figure 3.17 Typical launching method for dielectric rod using metal waveguide

Figure 3.17(b) is also a structure used for launching the dielectric rod. The cavity shown in the cut-away section is for matching. The match is facilitated greatly by the chamfering shown. Fig. 3.17(c) shows other two typical transition structures, less convenient for experiment work but affording somewhat better coupling from the metal to the dielectric waveguide.

❑ Coaxial cable

Coaxial cable can also be used to excite the dielectric rod as shown in Fig. 3.18.

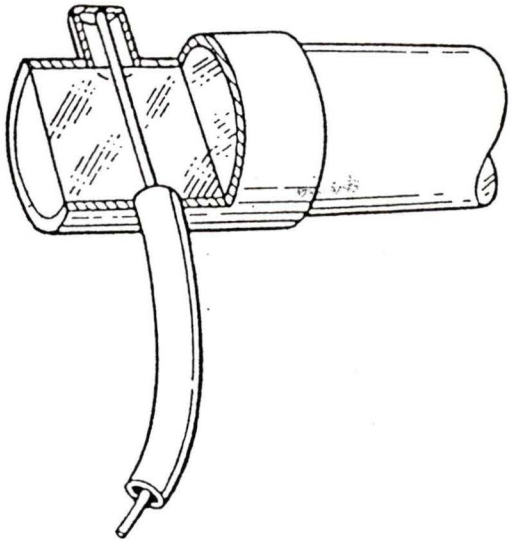

Figure 3.18 Coaxial cable launcher

3.3.2 Goubau line

The wave in the Goubau line can be launched with good efficiency by means of a device sketched in Fig. 3.19. The outer conductor of the coaxial feed line is gradually expanded in the form of a horn and the inner conductor of the line is connected to the surface waveguide. The device can be considered as a tapered coaxial line [23].

The best results were obtained with the launcher design shown in Fig. 3.19. The coaxial section has large diameter and the inner conductor is tapered down until it approximately matches the diameter of the Goubau line conductor.

The efficiency of the launching device of Fig. 3.19 can be determined approximately if the opening of the horn does not too much exceed the area within which the field decreases with 1/r. The efficiency is approximately equal to the ratio that the power which is in the range of the diameter of horn to the total power. It can be expressed as follows:

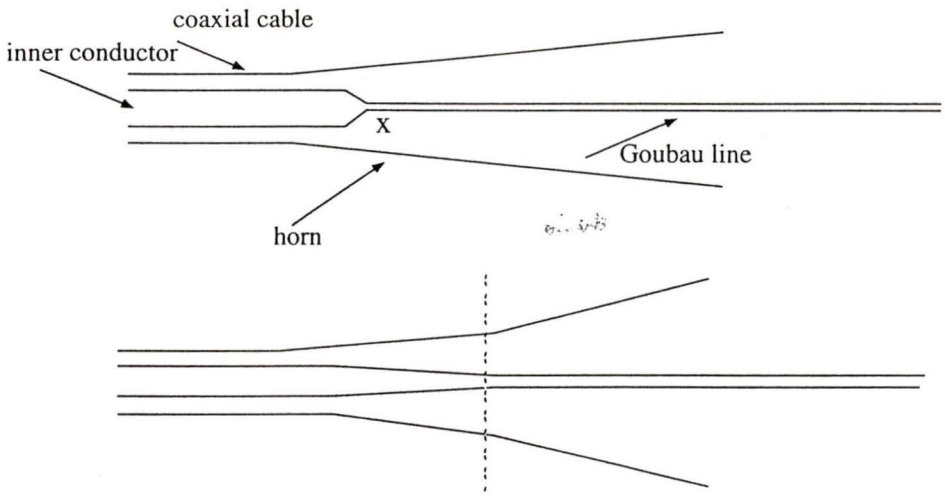

Figure 3.19 Launcher for Goubau line [23]

$$eff = 1 - \frac{F(h\rho)}{F(hb)} \tag{3.38}$$

where h is the eigenvalue of Goubau line,

ρ is the radius of horn, b is the outer radius of Goubau line and the function F is expressed by (3.31).

3.4 Comparison between surface waveguides and other transmission lines

In the previous sections, we presented the calculation of the propagation velocity, attenuation and effective diameter of the dielectric rod and the Goubau line which form the basis of the design of the surface waveguides as the transmission media for MLGS. For a microwave level gauging system, an ideal transmission medium should have following characters: 1) non-dispersive propagation; 2) small field extension; and 3) low attenuation. Follows will give the theoretical comparisons between surface waveguides and some other transmission structures. The comparisons will emphasize on three aspects: dispersion, field extension and attenuation.

❑ Dispersion

A distinguishing advantage of microwave techniques for level measurements is its capability of ignoring the disturbing objects around the liquid surface. Unfortunately, such capability is highly dependent on the technique used. It is regarded that FMCW technique has better resistance to the parasitic reflections because the sophisticated signal processing techniques can be applied to the obtained data and the undesirable reflections can be filtered out. For MFCW technique, the multiple reflections will cause inevitable measurement errors. The FMCW technique can only be applied to the non-dispersive transmission media. Thus, the dispersion of the transmission media directly determines the capability of ignoring the disturbing objects of the system. The propagation velocity of the free space, metallic waveguides and surface waveguides are shown in Fig. 3.20. The Goubau line is made of a 0.9 mm diameter copper wire coated with 1.03 mm teflon layer and the diameter of the teflon rod is 9.5 mm.

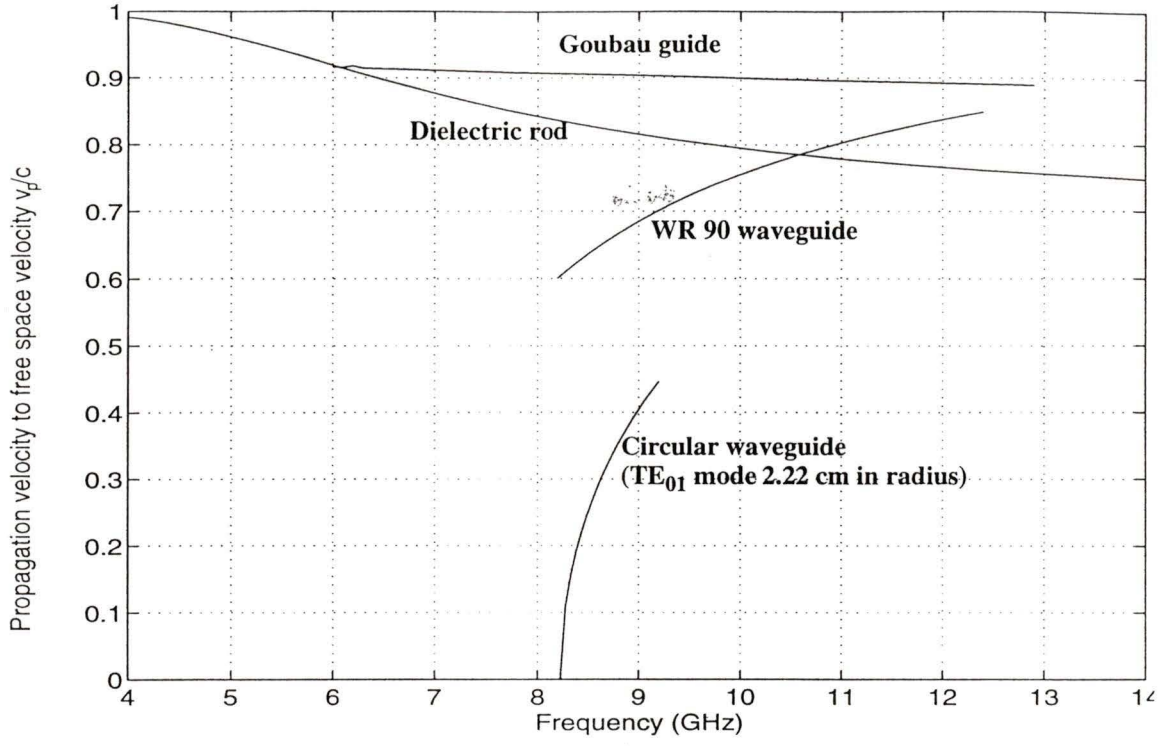

Figure 3.20 Propagation velocity of the Goubau line, the dielectric rod and metallic waveguides

From Fig. 3.20, we can see the Goubau guide shows almost non-dispersive character which make it possible to apply time domain techniques and FMCW technique to it.

❑ Field extension

For a closed boundary structure, the wave propagates within the structure. So, the physical dimension represents the field extension. However, for surface waveguides, part of the energy is transmitted outside the structure and therefore the effective diameter is much larger than physical diameter. The comparison of the field extension for coaxial cable, copper waveguides, dielectric rods and Goubau lines is shown in Fig. 3.21. The curves for coaxial cable and waveguides represent the dimension of the structures. For surface waveguides, the curves represent the effective diameters. The dielectric material for surface waveguides is teflon, whose dielectric constant is 2.08 and the loss tangent is 10^{-4}.

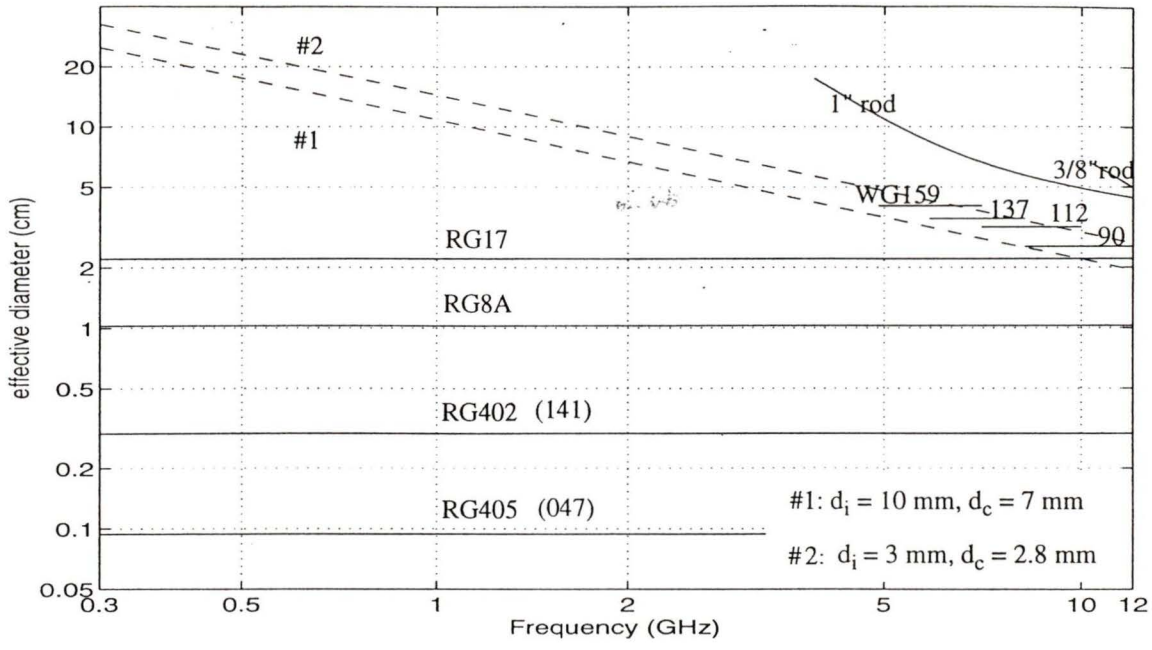

Figure 3.21 Comparison of field confinements

❑ Attenuation

Besides effective field volume, transmission losses are also of interest for the transmission medium. Figure 3.22 gives a comparison of the losses of coaxial cables, copper waveguides, dielectric rods and Goubau lines.

From Fig. 3.21, we can see that the effective volumes of surface waveguides, which are of interest in practice, are acceptable in the high frequency range. Although the transmission losses of surface waveguides increase with the increasing of operation frequency, they are still distinguishably smaller than coaxial cable and copper waveguides. Furthermore, for the Goubau line, the losses can be made even smaller than those shown in Fig. 3.22 since there is no limitation on the diameter of the conductor as far as modes are concerned.

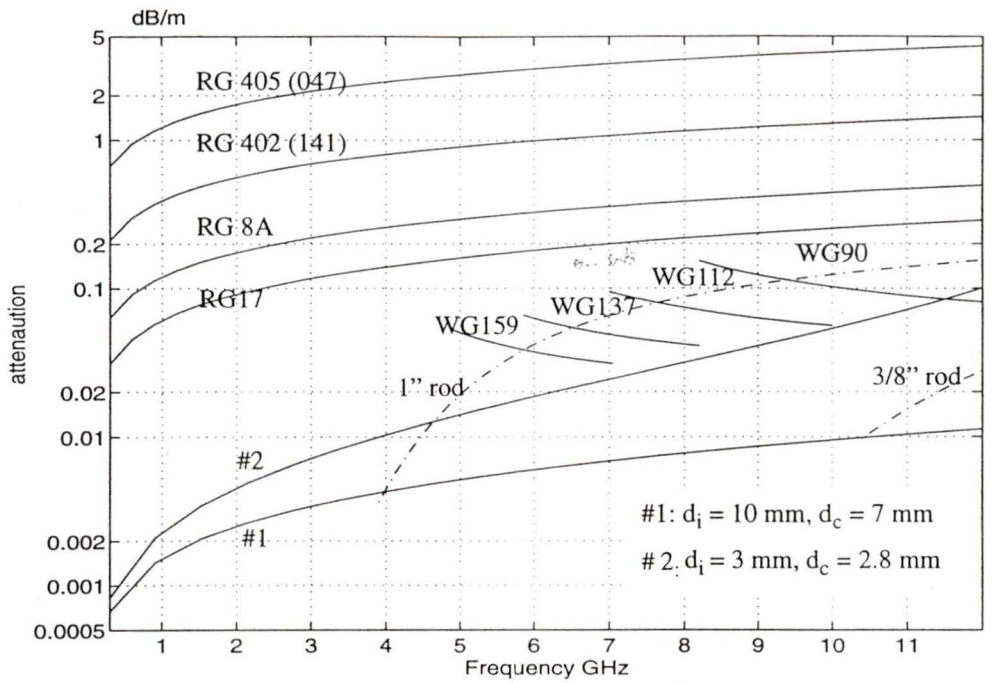

Figure 3.22 Attenuation of surface waveguides and other transmission media

Besides transmission losses and effective field volume, other factors including bandwidth, dispersion and ease of fabrication are also very important. Table 3.1 compares the surface waveguides and some common transmission media.

Table 3.1. Comparison between surface waveguides and some other common transmission lines

properties	coaxial cable	rectangular waveguide	circular waveguide	dielectric rod	Goubau line
modes: preferred	TEM	TE_{10}	TE_{11}, TE_{01}	HEM_{11}	TM_{00}
others	TE, TM	TE, TM	TE, TM	Hybrid, TE, TM	Hybrid, TE, TM
Dispersion	None	dispersive	dispersive	dispersive	dispersive
Attenuation	high	medium	very low	low	low
Bandwidth	high	low	low	high	high
Power capacity	medium	high	high	N/A	medium
Easy of fabrication	medium	medium	medium	easy	medium
Power confinement	excellent	excellent	excellent	good	poor
Magnitude of reflection (water-air)	high (0.8)	high (0.8)	high (0.8)	medium (0.5)	medium(0.4)

Chapter 4

System description and experimental results

In the previous chapters, we introduced the techniques for signal processing and two kinds of surface waveguides. In this chapter, we will investigate a scheme for a microwave level gauging system utilizing a surface waveguide as the transmission medium. The system arrangements as well as experimental results will be presented.

4.1 System

4.1.1 System scheme

Two kinds of transmission media have been adopted for microwave level gauging systems: free-space propagation and over-moded circular waveguide propagation. In those systems, there are several limitations which degrade the performance of the systems. The limitations can be attributed to following three factors:

1. Inevitable multiple reflections in the free space propagation system
2. Meniscus effect and deposits on the waveguide wall in the waveguide propagation system
3. Bulky hardware and difficulty in installation for the overmoded waveguide propagation system

Free-space propagation is free of meniscus effects and guided propagation can exclude the parasitic reflections. The ideal transmission medium for a microwave level

gauging system is a structure that combines the advantages of both free space and waveguides.

The open boundary surface waveguide appears to be an ideal structure. Firstly, the open boundary structure reduces the surface tension at the interface, which in turn reduces the meniscus effect. Secondly, the field extension of the surface waveguides can be confined within a small region around the structure so that the parasitic reflections from the surrounding objects can be avoided. In addition, the surface waveguide has a low transmission loss and a simple physical structure.

The proposed system uses a Goubau line or dielectric rod as the transmission media and a MFCW technique for the processor. The operation frequency ranges from 8.2 GHz to 12.4 GHz. Figure. 4.1 shows the system diagram.

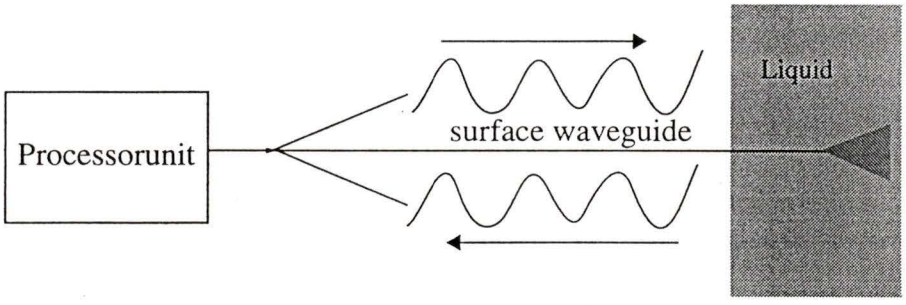

Figure 4.1 Scheme diagram of proposed system

4.1.2 System description

A microwave level gauging system with the proposed scheme was designed. Figure 4.2 illustrates the system arrangement.

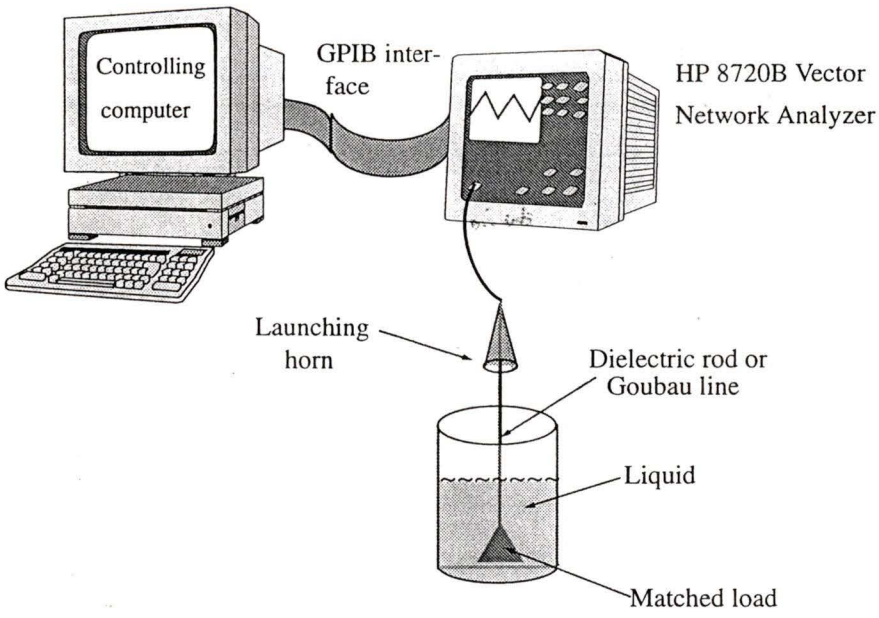

Figure 4.2 A microwave level gauging system with surface waveguide as the transmission medium

4.1.2.1 Processor unit

The processor for a microwave level gauging system executes three functions:

1. transmit an electromagnetic wave;
2. measure the reflection coefficient at the reference plane;
3. process the obtained reflection coefficient and get the level information

Usually, a processor consists of several microwave components. Figure 4.3 shows a simplified diagram of the processor.

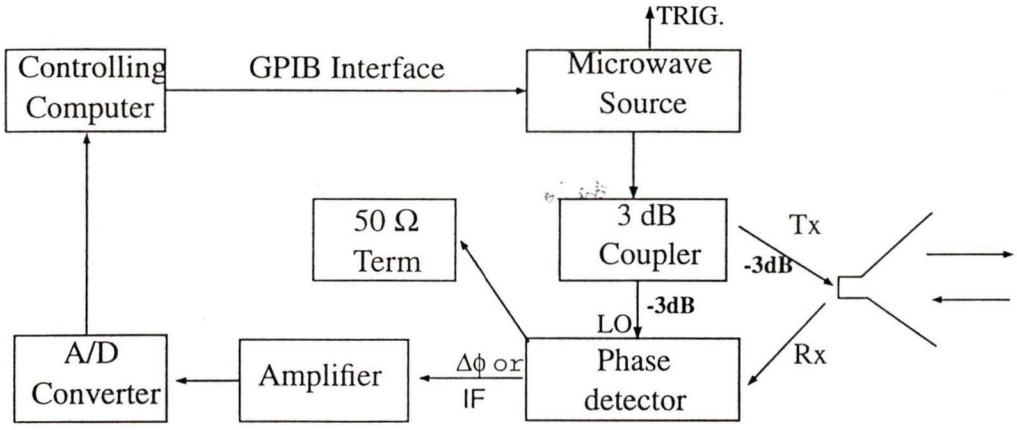

Figure 4.3 Diagram of the processor

From Fig. 4.3 we can see that the processor is very similar to a network analyzer. The forward reflection coefficient S_{11} obtained by the network analyzer provides an idealized model for the processor. Moreover, using a network analyzer, we avoid the use of a quadrature mixer which produces a hardware phase shift and causes measurement error. The results from the network analyzer will form a excellent model for the results obtained by the system shown in Fig. 4.3. In our experimental arrangements, a HP8720B vector network analyzer, which is connected with an IBM PC computer by GPIB interface, is used as the processor.

4.1.2.2 Transmission media

❑ Dielectric rod and Goubau line

For the transmission medium of the microwave level gauging system, mono mode operation is required. For the dielectric rod, the mono mode condition is expressed by (3.17). Since the operation frequency of the proposed system ranges from 8.2 GHz to 12.4 GHz, the cutoff frequency f_c of the HE_{11} mode should be greater than 12.4 GHz. From (3.16) and (3.17), we get

$$f_c = \frac{2.45c}{2\pi a\sqrt{\varepsilon_r - 1}} \geq 12.4GHz \tag{4.1}$$

where a is the radius of the rod and ε_r is the relative dielectric constant of the rod material and c is the velocity of light

If we choose teflon as the rod material, its dielectric constant is $\varepsilon_r = 2.08$, the diameter of the rod should satisfies

$$d \leq 1.82cm\ (0.72inch) \tag{4.2}$$

The teflon rod used for experiment was 3/8" in diameter. The cutoff frequency for HE_{11} mode is 23.6 GHz. The phase velocity, effective diameter and attenuation for the 3/8" rod are shown in Fig. 4.4

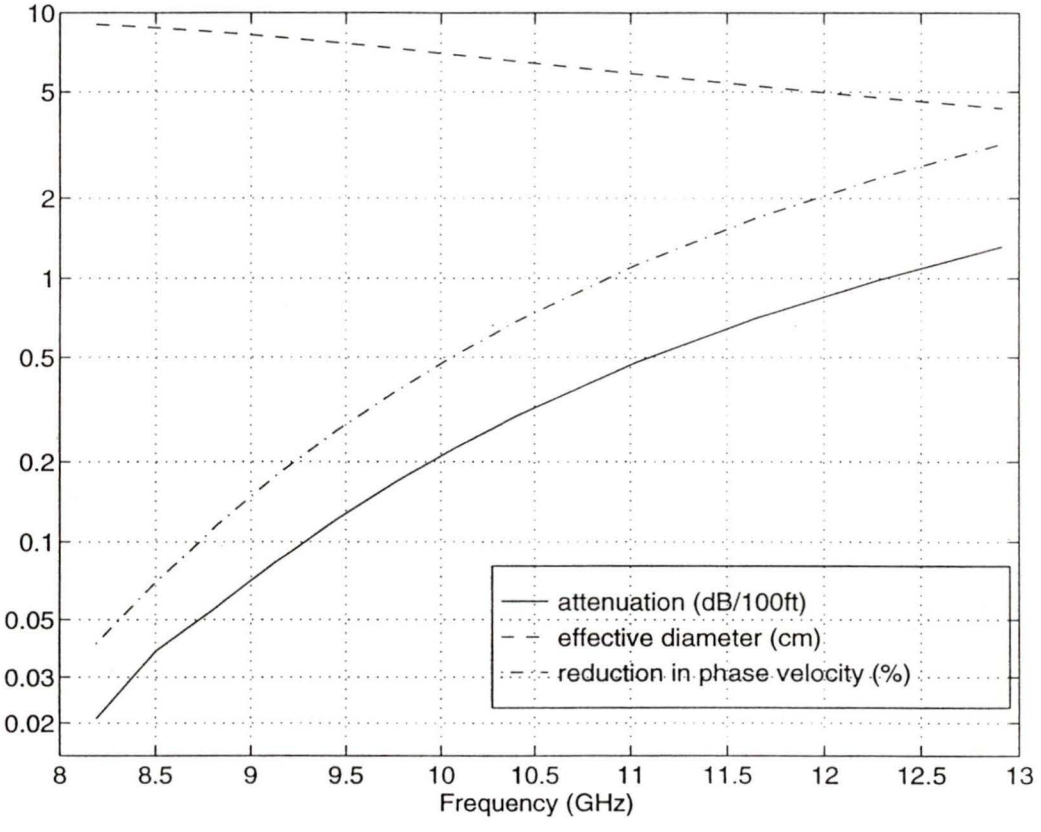

Figure 4.4 Parameters of the dielectric rod

For the Goubau line, there is no limitation on the dimension of the line as far as

modes are concerned. We choose a core diameter of 0.92 mm and a dielectric thickness of 1.03 mm. This is for the easy fabrication since the dimension is same as the dimension of 141 semi-rigid coaxial cable. The Goubau line can be made by simply stripping the outer conductor of the coaxial cable. The phase velocity, effective diameter and attenuation of the Goubau line are shown in Fig. 4.5.

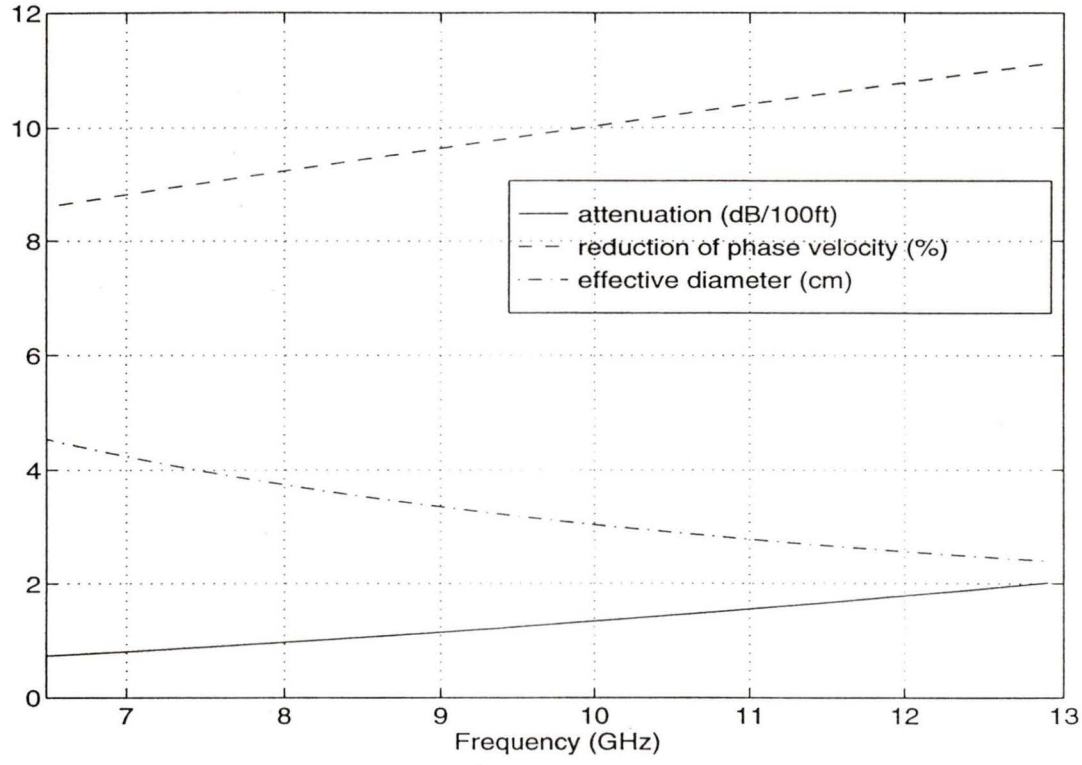

Figure 4.5 Parameters of the Goubau line

❑ Launching devices

To establish the proper mode in the surface waveguide, a launching device is required. From the discussion in Chapter 3, we know that high launching efficiency can be obtained if the launching device develops a field having a structure similar to that of surface wave within a cross section. For a practical system, other factors besides the launching efficiency, such as the bulkiness, ease of fabrication, and cost should also be

considered.

A rectangular horn is used as the launching device for the dielectric rod. The specifics are listed in Appendix A and the structure is shown in Fig. 4.6. The tapered section of the rod is to eliminate the reflection caused by the discontinuity at the interface of the rod and metal waveguide.

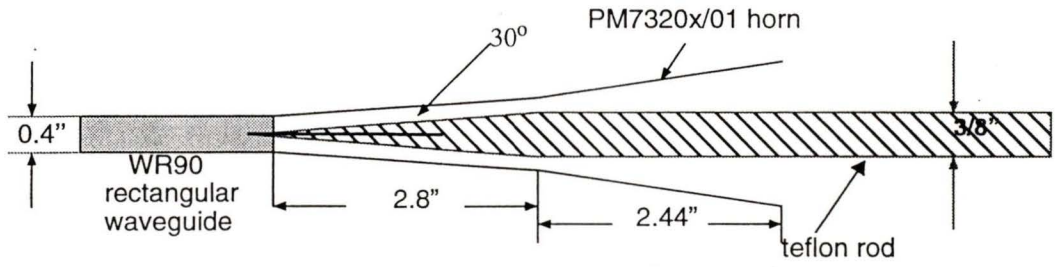

Figure 4.6 Launching structure of dielectric rod

For the Goubau line, the most efficient launching device is a kind of tapered coaxial line. That is, the inner conductor of the coaxial cable connects directly to the core of the Goubau line and the outer conductor expands gradually in the radius direction to form a horn. As the dimensions of the Goubau line are chosen to be the same as that of the 141 semi-rigid coaxial line, the most convenient horn is made of the 141 semi-rigid cable. An experimental structure is shown in Fig. 4.7. From Fig. 4.7, we can see that the teflon coated inner conductor of the launching coaxial cable extend outside and directly form the Goubau line. The outer conductor gradually expands to form a horn. Such arrangement avoids the connection between the coaxial line and the Goubau line and thus avoids a reflection at the connection.

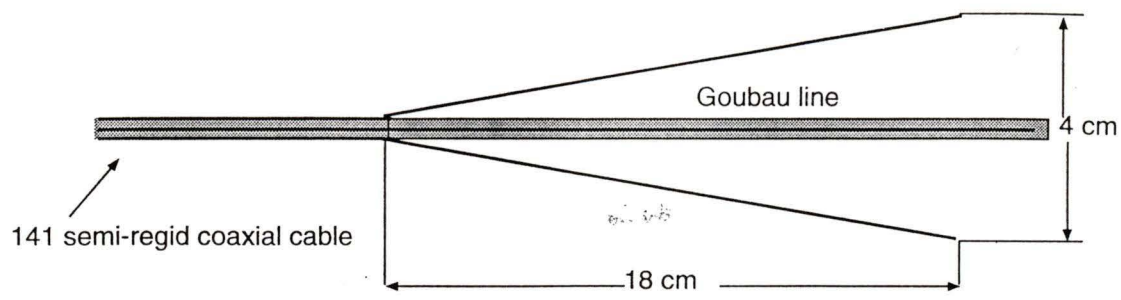

Figure 4.7 Launching structure for Goubau line

Also, from equation (3.38), we can get the approximate launching efficiency of the designed launching horn. The efficiency versus operation frequency is shown in Fig. 4.8. Here we should point out that Fig. 4.8 shows the launching efficiency for the ideal case. For the actual launching horn, there exist reflections which are caused by hardware imperfections and therefore the efficiency is lower than predicted.

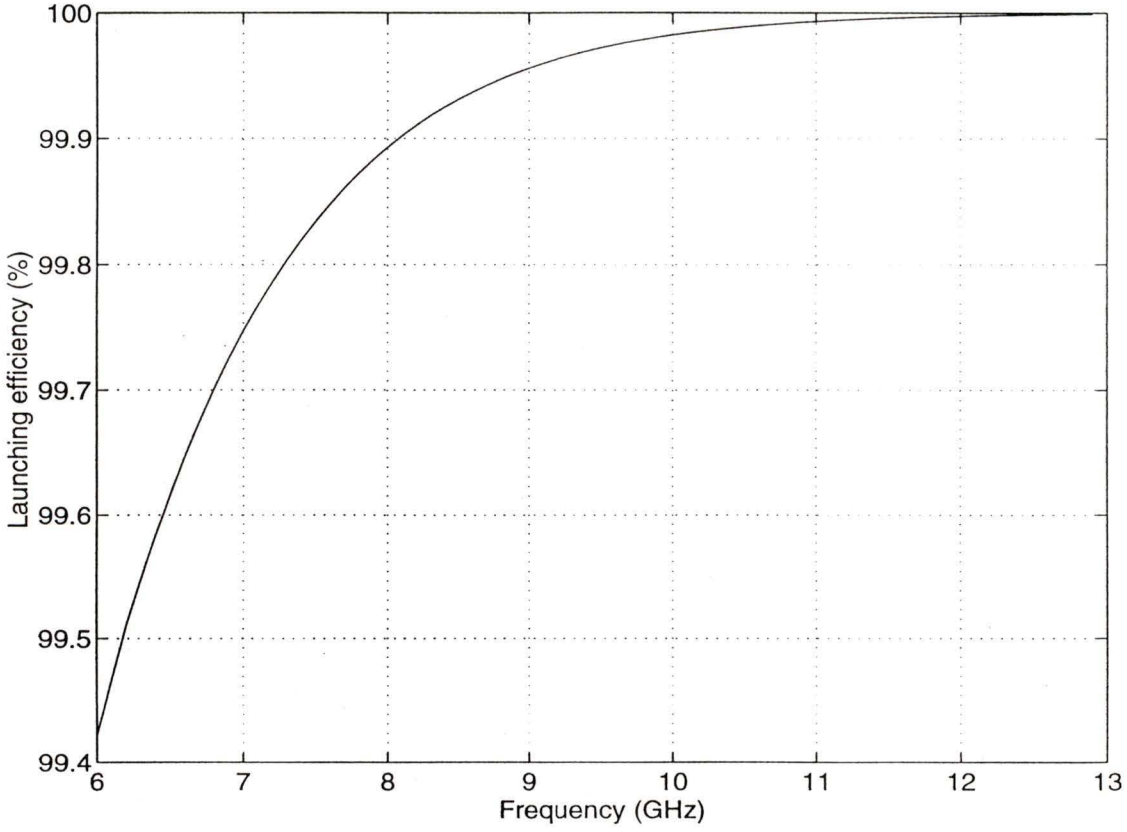

Figure 4.8 Launching efficiency of the Goubau line

❑ Termination

To avoid the reflection at the end of the surface waveguide, a matched load has to be used as the termination. Matched loads for the Goubau line and dielectric rod were designed. The loads were made of microwave absorbing casting silicon. The specifications for the microwave absorbing material is given in Appendix B. The structure of termination, together with the launching horn and the Goubau line, is shown in Fig. 4.9. The insertion loss at the termination is below -30 dB.

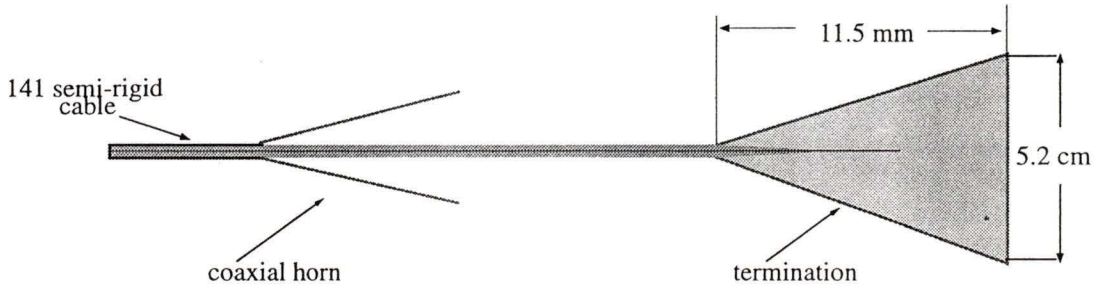

Figure 4.9 Structure of the transmission medium (Goubau line)

4.2 Experimental results

4.2.1 Objective of experiments

The objective of the experiments was to verify the feasibility of the proposed scheme. The experiments included two procedures:

1. verify the theoretical prediction of the effective diameter and transmission loss for the two surface waveguides
2. perform level measurement and evaluate the system performance

For the first procedure, a large number of experiments have been carried out by former workers [23] and the theoretical calculations have been proved to have good consistence with the experiment measurements. Therefore, our work emphasized the level measurement and evaluation of the system performance.

The measurements of water levels and oil levels were performed with the system using the Goubau line as the transmission medium. Both time domain technique as well as the MFCW technique were applied to obtain the level information.

4.2.2 Water level measurement

Figure 4.10 shows the time domain response of the system for the water level measurement. Figures 4.11 and 4.12 illustrate the magnitude and phase of the measured reflection coefficients when the frequency is swept from 8 to 12 GHz. The uneven level of the magnitude of the reflection coefficient is due to undesirable reflections from the surface wave launcher and the termination.

Measurements were performed for 10 different water levels and the MFCW technique was used to calculate the levels. The two operation frequencies of the MFCW technique are 10 GHz and 10.1 GHz. The measured water levels are shown in Fig. 4.13.

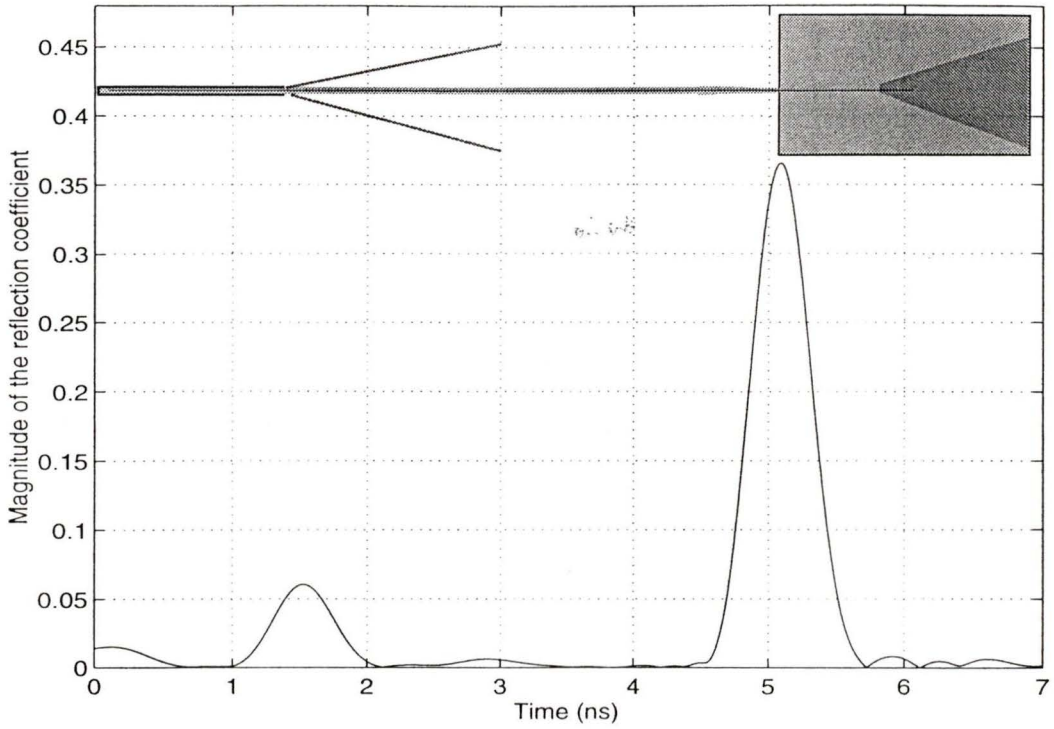

Figure 4.10 Time domain response of the system for water measurement.

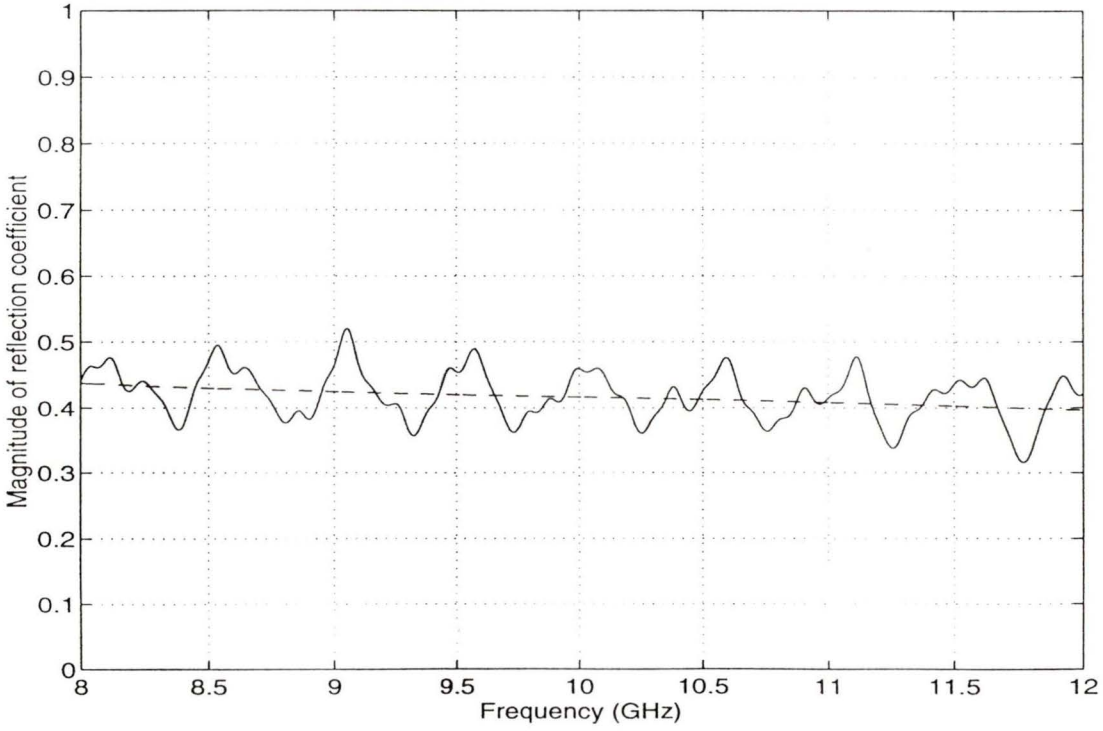

Figure 4.11 Magnitude of the reflection coefficient

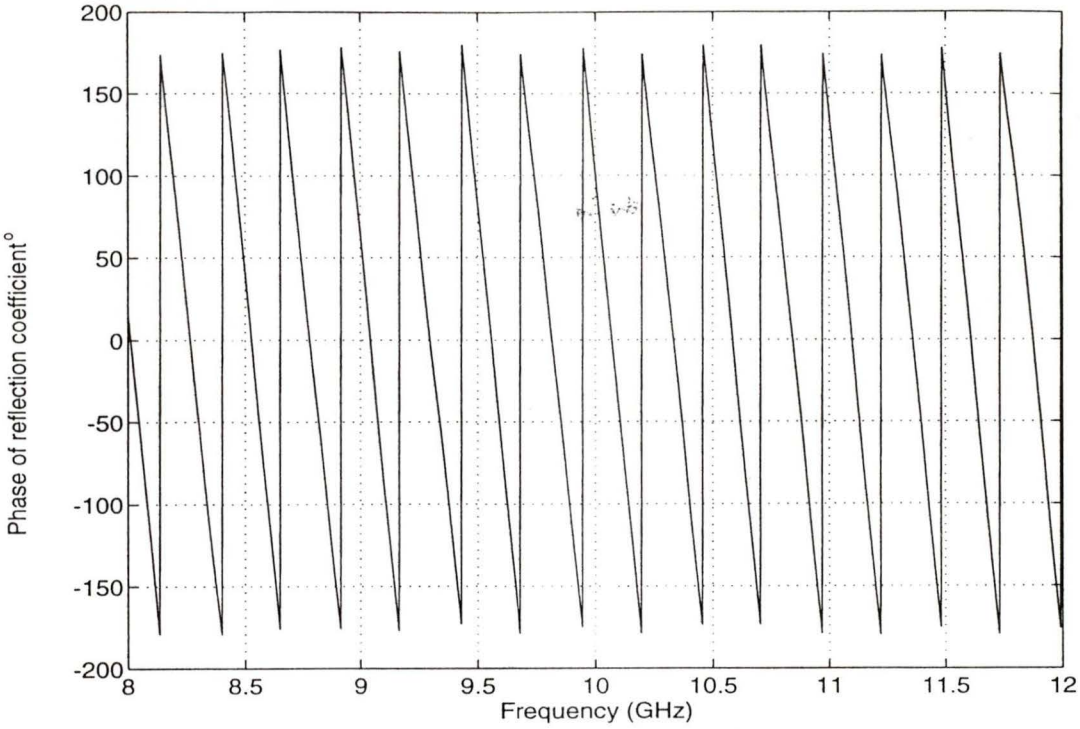

Figure 4.12 Phase of the reflection coefficient

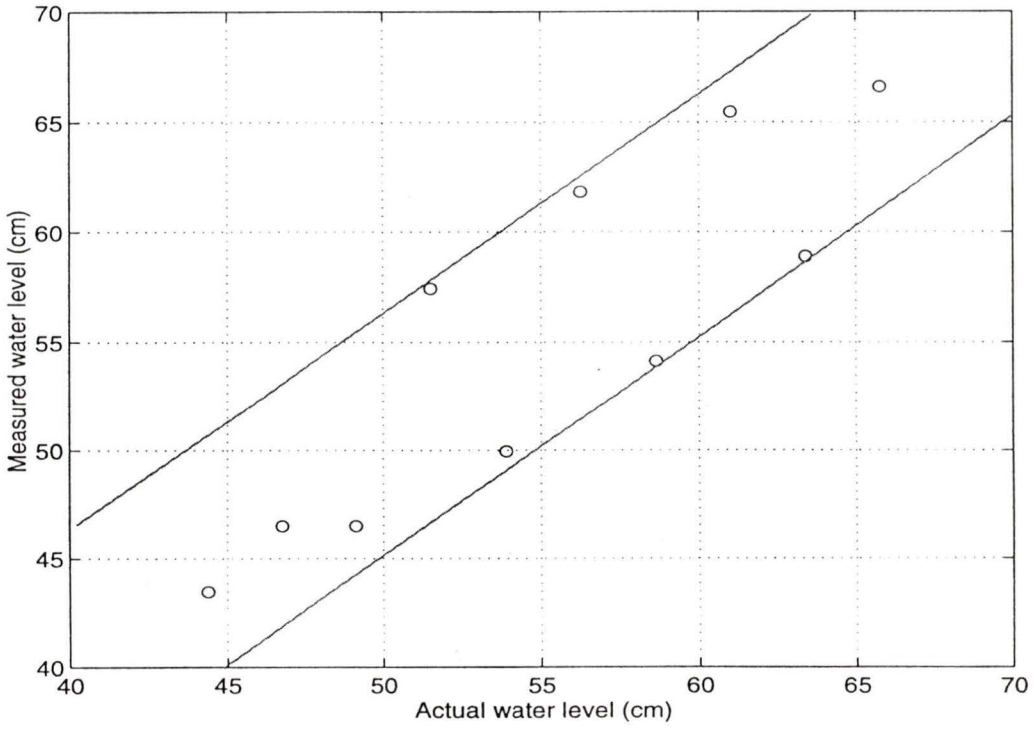

Figure 4.13 Measured water levels

4.2.3 Oil level measurement

Figure 4.14 shows the time domain response of the system for oil level measurement. Figures 4.15 and 4.16 shows the magnitude and phase of the measured reflection coefficients when the frequency is swept from 8 GHz to 12 GHz. Similar to that in water level measurements, the level measurements were also performed at 10 different oil levels and the MFCW technique was applied to obtain the level information. Figures 4.17 shows the result of the measurements.

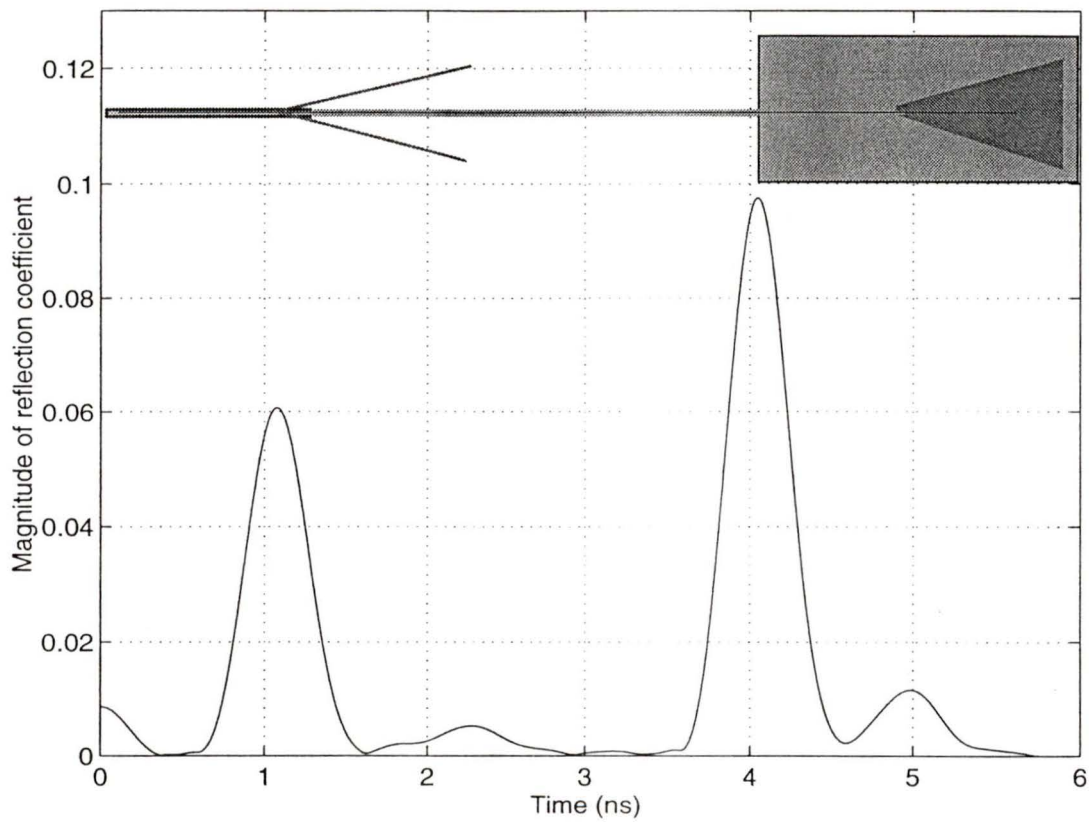

Figure 4.14 Time domain response of the system for oil level measurement

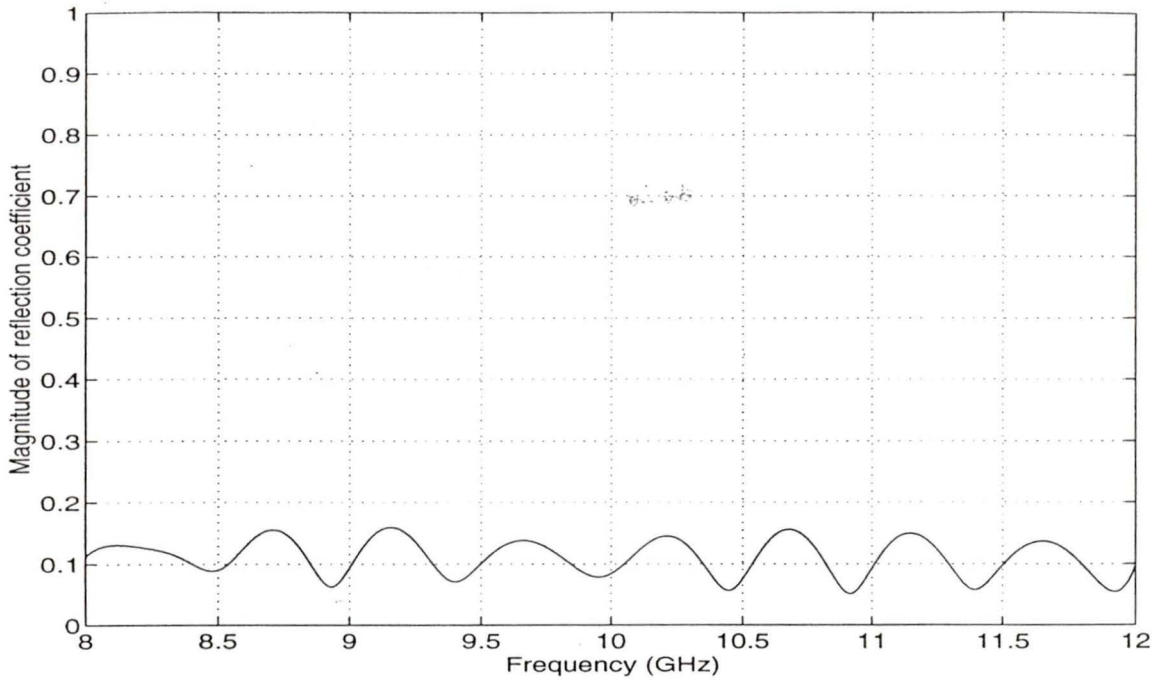

Figure 4.15 Magnitude of the reflection coefficient

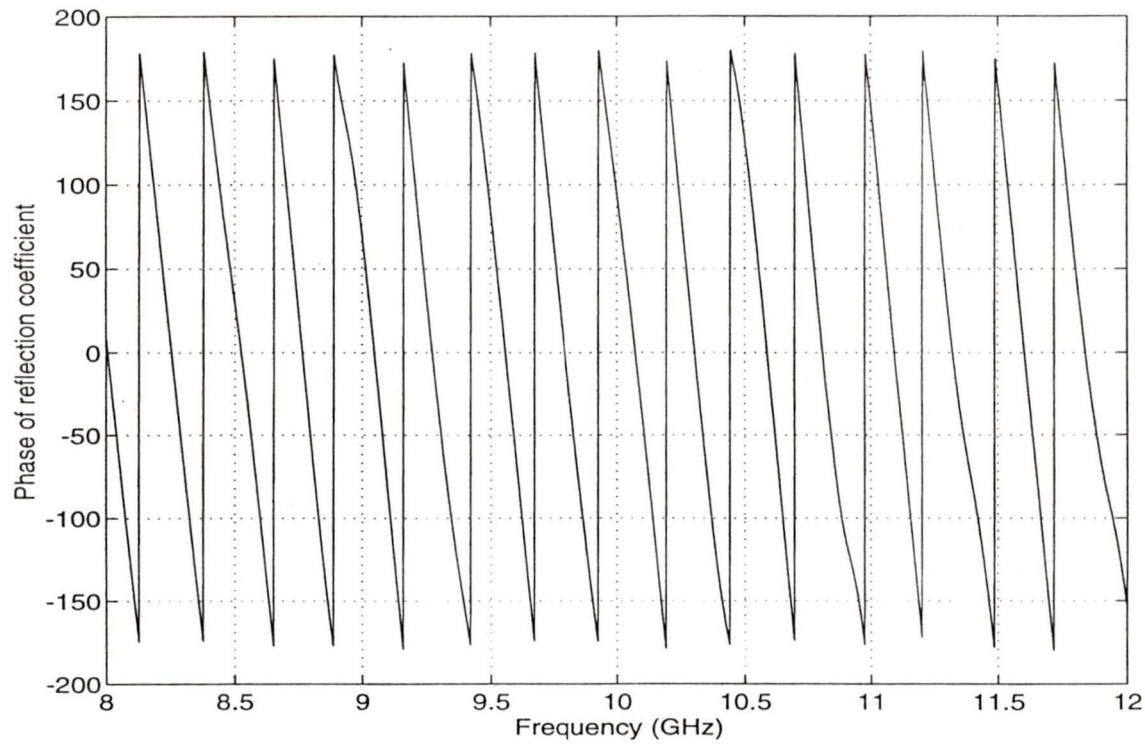

Figure 4.16 Phase of the reflection coefficient

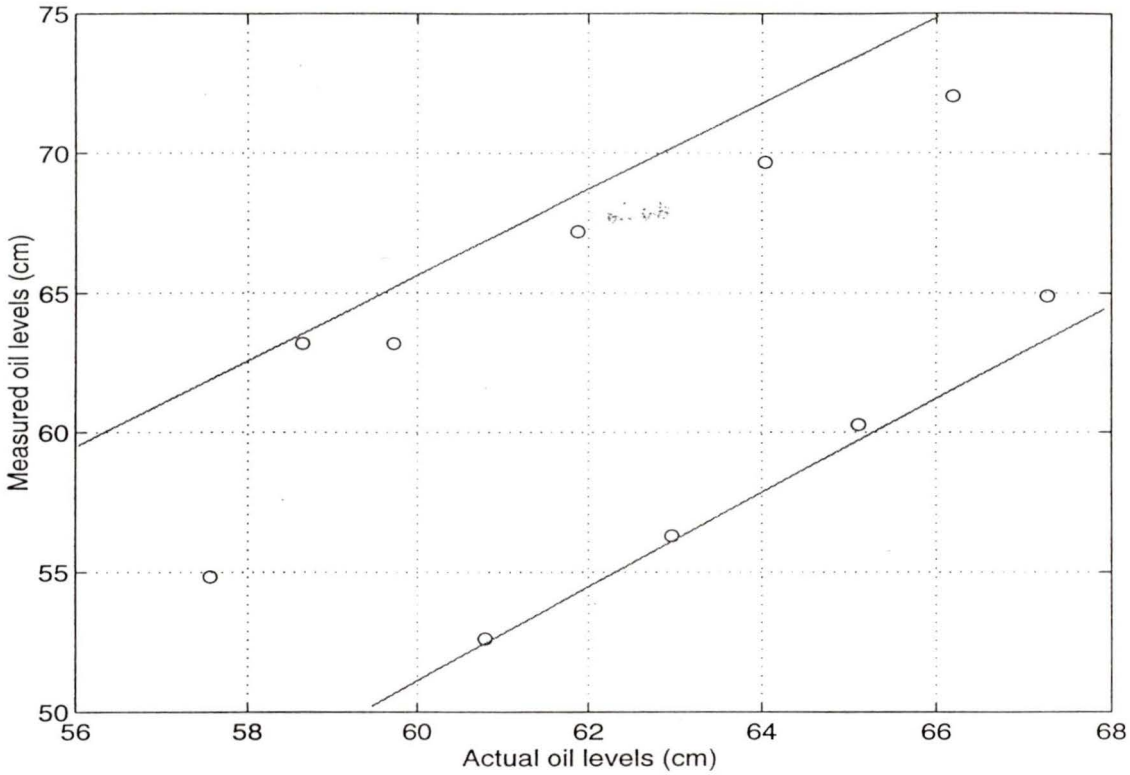

Figure 4.17 Measured oil levels

4.2.4 System accuracy analysis

From Fig. 4.13 and 4.17, we can see that the measured levels of the test liquids with MFCW technique have a large deviation from the actual levels of the liquids. These large measurement errors consist of three parts:

1. the errors caused by the uncertainty in the processor unit
2. the errors caused by the changes in the processing environment
3. the errors caused by the imperfection of the transmission medium

4.2.4.1 Uncertainty in the processor unit

In Chapter 2, it was shown that with MFCW technique, the level can be expressed as

$$R = \frac{v\Delta\phi}{4\pi\Delta f} \tag{4.3}$$

where v is the propagation velocity, $\Delta\phi$ and Δf is the phase difference and frequency difference respectively. Taking the partial derivative of (4.3) we can find the effect of variations in the parameters involved on the level measurement, i.e.,

$$\delta R = \frac{\Delta\phi}{4\pi\Delta f}\delta v + \frac{v}{4\pi\Delta f}\delta(\Delta\phi) + \frac{v\Delta\phi}{4\pi(\Delta f)^2}\delta(\Delta f) \tag{4.4}$$

where δR is the uncertainty of the level measurement and
δv, $\delta(\Delta\phi)$ and $\delta(\Delta f)$ are the variation in the propagation velocities, phase measurement and frequency difference, respectively.

The first term on the right hand side of (4.4) depends on the changes in the propagation velocity. The second term depends on the uncertainty of the phase measurement while the last term is determined by the stability of the frequency generator. It is also obvious from (4.4) that an large Δf is desirable to reduce the effect of variation of the parameters and thus to increase the accuracy of the level measurement.

In the proposed system, since a vector network analyzer was used as the processor, the stability and accuracy of the frequency of the transmitted signal is very high, e.g. 7.5 ppm for HP8720C NA. The operation frequency can be regarded as a constant during the measurement and therefore the effect of the third term in (4.4) is negligible.

As to the variation in phase measurement, for HP 8620C NA, the uncertainty of phase measurement within the operation frequency range is about 4^{o}. If one of the carrier frequency was used to obtain the final level of the liquid (See "FM-CW technique" on page 25.), the measurement error caused by the 4^{o} phase shift is 0.15 mm which is also negligible in the measurements.

4.2.4.2 Variation in the processing environment

As discussed in Chapter 3, the propagation velocity of the surface waveguide is determined by the propagating mode, operation frequency and the dimension of the surface wave structure. For example, the propagation velocity v for the Goubau line can be written as

$$\frac{2\pi f}{v} = \sqrt{\left(\frac{2\pi f}{c}\right)^2 + h^2} \tag{4.5}$$

where f is the operation frequency, h is the eigenvalue which depends on the operation frequency as well as dimension of the structure, and c is the velocity of free space propagation.

Since the operation frequency was very stable in the proposed system, the change in the dimension of the structure is the only factor which may affect the propagation velocity. For the Goubau line and the dielectric rod, the change in the dimension is usually caused by change in the ambient temperature. However, it is very difficult to quantitatively evaluate the effect of the variation in the ambient temperature on the propagation velocity. For the measurements which were carried out in our lab, the change of the temperature is very small. It is reasonable to assume that the dimensions of the surface waveguide remain constant during the measurements and therefore the actual wave propagation velocity is the same as the theoretical prediction and do not introduce measurement error to the final liquid level measurements.

4.2.4.3 Imperfection of the transmission medium

From the above discussions, we can see that in our system, the processor used and the processing environment do not introduce significant measurement errors in liquid level. Another reason of error are the imperfections of the transmission medium.

As discussed in Chapter 2, for the MFCW technique, the processor transmits two

signals whose frequency is slightly different to obtain the level information. If there is only one reflective target, the MFCW technique can give accurate distance measurement between the transmitter and the target. However, if more than one reflective targets exist, the measurements are severely disturbed.

For example, if there is an object between the transmitter and liquid surface for the level measurement of liquid, assuming the distance from the transmitter to the object and liquid surface is R_1 and R, and the two transmitted signals are

$$V_{t1} = sin 2\pi f_1 t \tag{4.6}$$

$$V_{t2} = sin 2\pi f_2 t \tag{4.7}$$

The echo signals received at the receiver are

$$\begin{aligned} V_{r1} &= sin\,[2\pi f_1 (t - 2R_1/v)] + sin\,[2\pi f_1 (t - 2R/v)] \\ &= 2\,sin\,[2\pi f_1 (t - (R_1 + R)/v)]\, cos\,[2\pi f_1 ((R_1 - R)/v)] \end{aligned} \tag{4.8}$$

$$\begin{aligned} V_{r2} &= sin\,[2\pi f_2 (t - 2R_1/v)] + sin\,[2\pi f_2 (t - 2R/v)] \\ &= 2\,sin\,[2\pi f_2 (t - (R_1 + R)/v)]\, cos\,[2\pi f_2 ((R_1 - R)/v)] \end{aligned} \tag{4.9}$$

where v is the propagation velocity of the transmitted signal

Applying the MFCW technique to the transmitted and received signals, we can get

$$\frac{R + R_1}{2} = \frac{v\Delta\phi}{4\pi\Delta f} \tag{4.10}$$

where Δf is the frequency difference and $\Delta\phi$ is the phase difference. Thus, due to the existence of the disturbing object, the MFCW technique gives the average of the distance from the transmitter to the disturbing object and the distance from the transmitter to the liquid surface. The measurement error is

$$\delta R = \frac{|R - R_1|}{2} \tag{4.11}$$

which is proportional to the distance between the disturbing object and liquid surface.

From the time domain response of the proposed system for water and oil level measurements (Fig. 4.10 & 4.14), we can see that there are two disturbing reflections in the measurements, caused by the surface waveguide launcher and the termination, respectively. In order to eliminate these disturbing reflections, a time domain window was applied to the received echo signal which filters out the reflections from the launcher and termination. Figure 4.18 shows the time domain response before and after applying the time domain window for the oil level measurement.

Figure 4.19 and 4.20 shows the measured results obtained with the MFCW technique. We can see that the measured levels of the test liquids are consistent with the actual level very well.

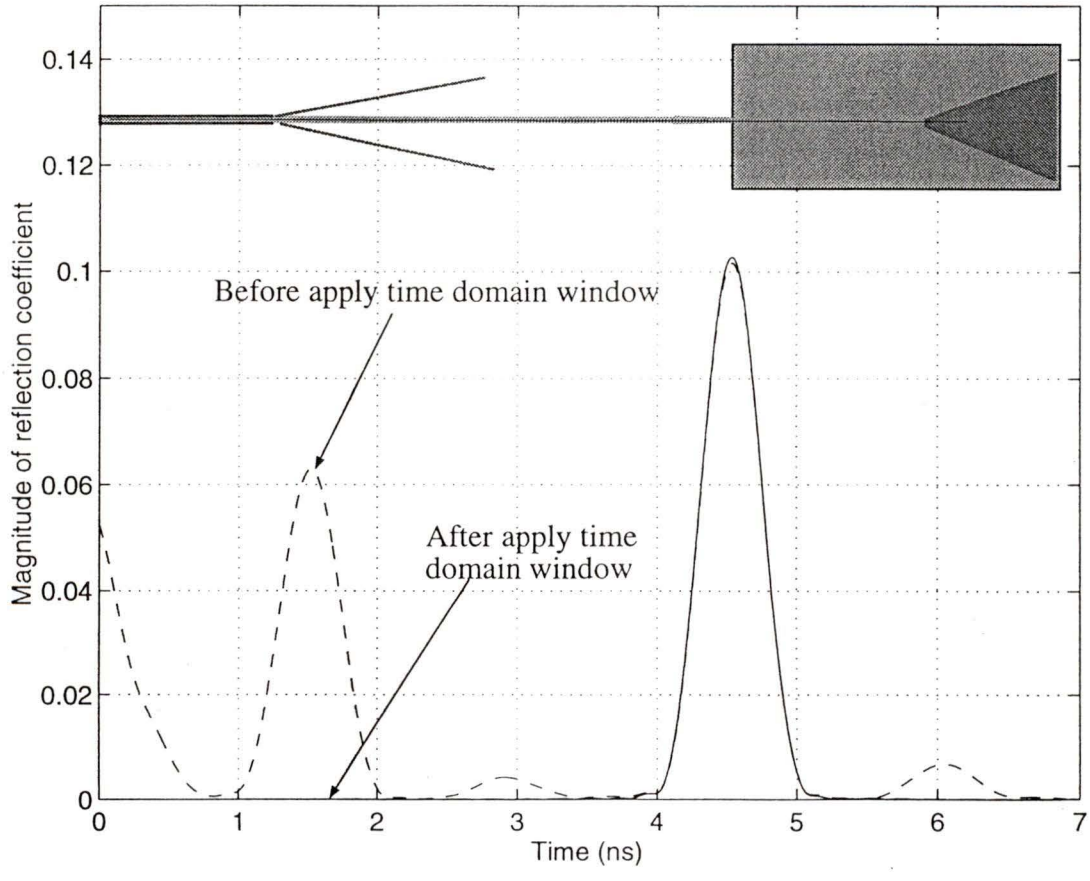

Figure 4.18 The time domain response for oil level measurements (before and after applying the time domain window)

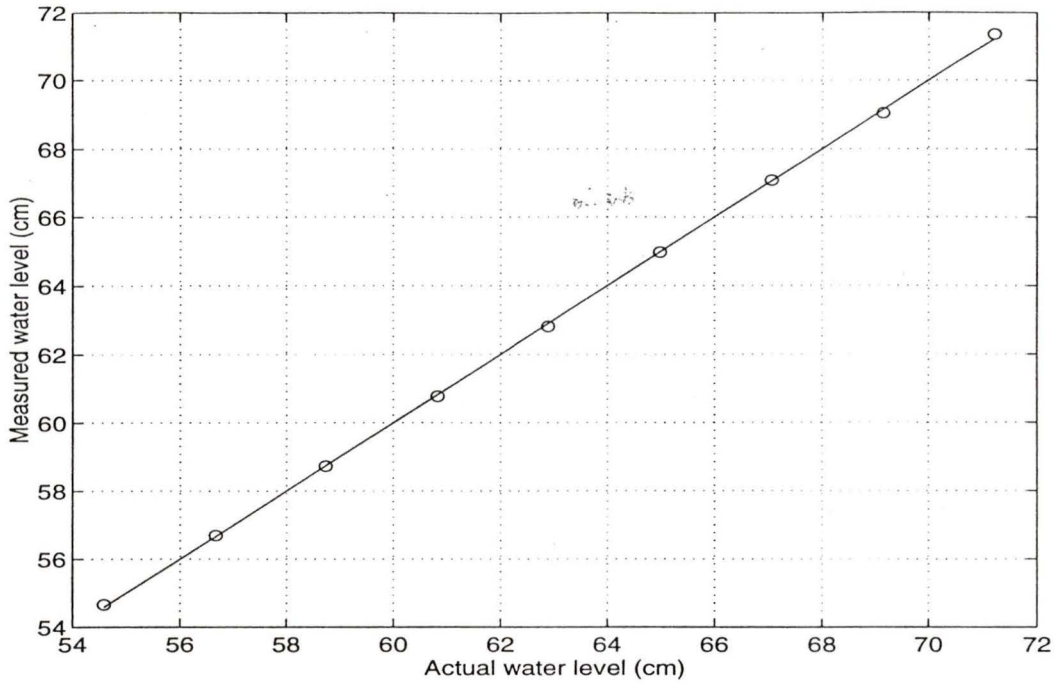

Figure 4.19 Measured water levels after applying the time domain window to the echo signal

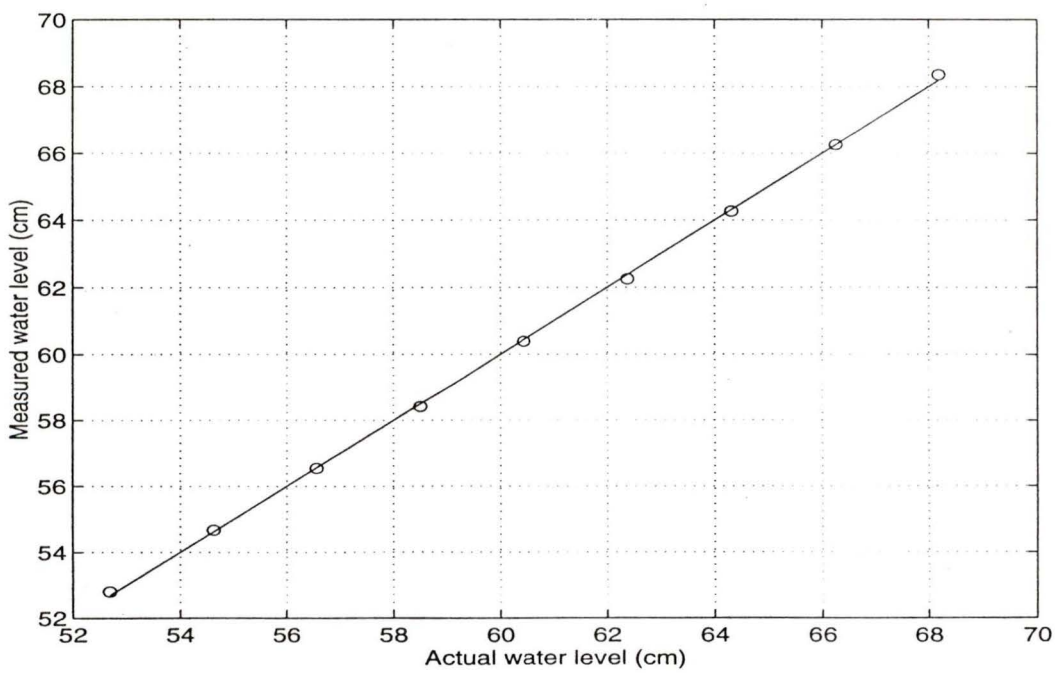

Figure 4.20 Measured oil levels after applying the time domain window to the echo signa

From the above discussions and experimental results, it is obvious that the network analyzer and the processing environment do not introduce any major measurement errors to the level measurements of the test liquids. The dominant error factors are the imperfection of the surface waveguide launcher and the termination for the surface waveguides. Therefore, in order to improve the measurement accuracy of the system, the reflections from the surface launcher and termination have to be reduced and an advanced launcher and termination are required.

Chapter 5

Conclusions

The major objective of this thesis was to investigate the feasibility of using surface waveguides as the transmission media for a microwave level gauging system. In this work, the microwave techniques for the level measurements were reviewed. Two kinds of surface wave structures, the Goubau line and the dielectric rod, were investigated as possible transmission media for the microwave level gauging system. The design of the Goubau line and the dielectric rod were presented and an experimental system with the proposed scheme was developed and the operation of the system was verified by measuring water and oil levels in a tank.

The time-domain technique and the MFCW technique were applied to obtain the liquid levels. For the time domain technique, the measurement results were in good agreements with the actual water levels. However, for the MFCW technique, the results did not agree with the actual levels very well. This is because in the measurements, the undesirable reflection component caused by the surface wave launcher and the termination in the echo signal disturbed the measurements. In order to improve the measurement accuracy of the system, a properly designed surface wave launcher and a low reflecting termination is required.

The features of the surface waveguides used as the transmission media for the microwave level gauging system can be summarized as follows:

1. Surface waveguides can avoid the parasitic reflections from the surrounding objects.
2. The contact of the liquid with the surface of the surface waveguide is resistant to deposits.
3. Within the frequency range of operation, the Goubau line and the dielectric rod show very little dispersion. Therefore, both time-domain as well as frequency-domain microwave level gauging techniques can be applied to the system. By using time domain techniques and swept-frequency techniques, we can apply sophisticated signal processing techniques to the echo signal, thereby excluding the undesirable components and improving the measurement accuracy.
4. The transmission losses of the Goubau line and dielectric rod are much smaller than those of metal waveguides, so the echo signal will be less attenuated and the SNR at the receiver will be greater than that in the circular waveguide system. Large SNR is also helpful in improving the measurement accuracy.
5. It has simple hardware, is easy to fabricate and easy to install.

There are, of course, some limitations of the system utilizing surface waveguides as the transmission media. First, in order to excite the desired mode along the transmission medium, a relatively complex launching device is needed. This launching device produces some inevitable reflections which contribute to measurement errors. To eliminate those reflections, a better designed surface launching device is required. Second, since the reflection from the termination causes severe measurement error, it requires a non-reflective termination which is rather difficult to manufacture. Moreover, the dielectric rod is not mechanically rigid or any bends on the Goubau line and the dielectric rod may induce measurement errors.

In general, through the theoretical and experimental studies, surface waveguides

have been proven to be feasible for a microwave level gauging system. The system with the Goubau line as the transmission medium has been successfully applied to measure the levels of water and oil in a tank.

Since the uncertainty of the level measurement depends on the reflections in the system, future work should emphasize improvements of the reflection at the liquid surface and reduction of the reflections from the launching devices and terminations for both surface waveguides. The future project may include: (1) the analysis of the launching devices for surface waveguides, including design of a simple, high efficiency launcher; (2) the design of a non-reflective termination for surface waveguides. Moreover, the work may emphasize applications of other techniques for microwave level gauging systems and signal processing techniques. By using computer signal processing techniques, it is possible to avoid the calibration and the critical requirement for the termination. In addition, it is also suggested to investigate other surface waveguides which have simple launching device, simple construction, and are mechanically solid, e.g. an image line.

Bibliography

[1] D. M. Considine, *Process Instruments and Controls handbook*, third edition, McGraw-Hill, 1985.

[2] W. W. Oglesby, "Radar Measures Sticky Liquid Level," *Instrumentation Technology*, Dec. 1991, pp36 -- 38.

[3] D. Farrant, "Radar Measurement is on the Level," *Control and Instrumentation*, Sep. 1992, pp55 -- 57.

[4] S. S. Stuchly, M. A. Hamid and A. Andres, "Microwave Surface Level Monitor," *IEEE Trans. Ind. Electron. and Control Instrum.*, vol. **IECI**-18, no. 3, Aug. 1971, pp85 -- 92.

[5] F. Gardiol, *Introduction to Microwaves*, Massechutte, Artech House, 1984.

[6] E. A. Wolff and Roger Kaul, *Microwave Engineering and System Applications*, New York, John Wiley & Sons, 1988.

[7] "Time Domain Reflectometry," *Application Note 62*, Hewlett-Packard Company

[8] L. R. Moffitt, "Time-Domain Reflectometry Theory and Applications," *Application Note 75,* Hewlett-Packard Company.

[9] M. I. Skolnik, *Introduction to Radar Systems,* New York, McGraw-Hill, 1962.

[10] G. S. Woods, D. L. Maskell and M. V. Mahoney, "A high Accuracy Microwave Ranging System for Industrial applications," *IEEE Trans. Intrum. Measur.* vol. **IM**-42, no. 4, August 1993

[11] S. Kobayashi, K. Katohgi, and A. Hatono, "Measurement of the slag level in BOF Using Microwave," 1981 **IMPI** Symposium, Toronto, June 1981.

[12] C. J. Kikkert and G. S. Woods, "The Measurement of Molten Metal Levels during Casting," *in 1992 Asia-Pacific Microwave Conference,* Adelaide, pp. 867--870.

[13] J. Detlefsen, "Frequency Response of Input Impedance Implies the Distribution of Discontinuities of a Transmission-line System," *Electron. Lett.*, vol. 6, Feb. 1970, pp. 67--69.

[14] D. A. Noon, "A Computer Controlled Microwave Distance Measuring System," *BE Thesis Dissertation*, Dept. Elec. Eng., Univ. Queensland, Australia, Oct. 1991.

[15] R. E. Collin, *Field Theory of Guided Waves*, New York, McGraw-Hill, 1960.

[16] D. Kajfez, and P. Guillon, *Dielectric Resonators*, Artech House, Inc., 1986.

[17] C. H. Chandler, "An Investigation of Dielectric Rod as Wave Guide," *J. Appl. Phys.* **20**, Dec. 1949, pp 1188 - 1192.

[18] W. M. Elsasser, "Attenuation in a Dielectric Circular Rod," *J. Appl. Phys.* **20**, Dec. 1949, pp 1193 - 1196.

[19] D. D. King, "Circuit Components in Dielectric Image Lines," *IRE Trans. Microwave Theory Tech.*, vol. **MTT-3**, March 1955, pp. 75 - 81.

[20] S. P. Schlesinger and D. D. King, "Losses in Dielectric Image Lines," *IRE Trans. Microwave Theory Tech.*, **MTT-5**, Jan. 1957, pp. 31 - 35

[21] G. Goubau, "Designing Surface-Wave Transmission Lines," *Electronics*, April 1954, pp 180 - 184.

[22] R. E. Collin, *Foundation for Microwave Engineering*, New York, McGraw-Hill, 1966.

[23] G. Goubau, "Surface Wave and Their Application to Transmission Lines," *J. Appl. Phys.* **21**, Nov. 1950, pp 1119 - 1128.

[24] R. H. Duhamel, and J. W. Duncan, "Launching Efficiency of Wires and Slot for a Dielectric Rod Waveguide," *IRE Trans. Microwave Theory Tech.*, vol. **MTT**- 6, July, 1958, pp. 277 - 284.

[25] H. Josik, *Antenna Engineering Handbook*, New York, McGraw-Hill, 1961.

[26] A. W. Rudge, K. Milne, A. D. Olver, and P. Knight, *Handbook of Antenna Design*, London, Peter Peregrinus Ltd., 1986.

[27] G. Goubau, "On Excitation of Surface Waves," *Proc. IRE*, vol. **40**, July 1952, pp 865 - 868.

Appendices

Appendix A

Specifications of PM 7320X/01 Rectangular Horn

- Frequency range: 8.2 GHz -- 12.4 GHz
- Midband gain: 16 dB
- VSWR: 1.25
- Waveguide: WR90
- Flange: Mate UBR 100
- Length: 133 mm
- Opening: 50 x 73 mm

Appendix B

Specifications of the C-RAM "KRS" Casting Silicone for Radar Absorbers

C-RAM "KRS" is a series of two part liquid RTV silicone casting resin kits which can be used to mold waveguide terminations, attenuators, loads, RF gaskets, and other radar absorber parts. when cured, the material converts to a flexible high temperature silicone rubber.

The KRS series will adhere to themselves, however, it will release from most other substrates.

Typical Cured Properties	KRS-124	KRS-117	KRS-116
Specific Gravity	4.55	4.2	3.7
Thermal Expansion	33 x 10	35 x 10	36 x 10
Thermal Conductivity	7	6	5.5
(BTU) (in) / (hr) (sqft) (F)			
Hardness shore A	75	75	75
Service Temp. Max. F	500	500	500
Water Absorption, 24 hrs	<0.1%	<0.1%	<0.1%
Dielectric Strength (Volts/mil)	> 25	< 25	> 25
Attenuation in Db/cm			
1.0 GHz	6.0	2.8	1.3
3.0 GHz	20.0	11.0	5.0
10.0 GHz	69	55	31

Table B.1 Specifications of the microwave absorber

VITA

Surname: Guo Given Names: Wei

Place of Birth: China Date of Birth: April 12, 1969

Educational Institutions Attended:

Tsinghua University	1987 -- 1992

Degrees Awarded:

B. Eng	Tsinghua University	1992

Honours and Awards:

University of Victoria	Reasearch Assistantship	1993 -- 1994

Publications:

(1) W. Guo, S. Stuchly and K. Caputa, "Microwave Level Gauging System", in 1994 IEEE AP-S International Symposium and URSI Radio Science Meeting, Seattle, Washington, USA, June 19 -- 24, 1994.

(2) W. Guo, M. Okoniewski, E. Okoniewska, and M. Bialkowski, "FDTD Analysis of a Goubau Waveguide Immersed in Liquid", submitted and accepted in Proc. ICCEA'94, Beijing, China, Nov. 1 - 4, 1994.

PARTIAL COPYRIGHT LICENSE

I hereby grant the right to lend my thesis to users of the University of Victoria Library, and to make single copies only for such users or in response to a request from the Library of any other university, or similar institution, on its behalf or for one of its users. I further agree that permission for extensive copying of this thesis for scholarly purposes may be granted by me or a member of the University designated by me. It is understood that copying or publication of this thesis for financial gain shall not be allow without my written permission.

Title of Thesis: MICROWAVE LEVEL GAUGING SYSTEM

Author [redacted]

(Signature)

WEI GUO

(Name in Block Letters)

Nov. 30, 1994.

(Date)